FISEVIER

Contents lists available at ScienceDirect

Commun Nonlinear Sci Numer Simulat

journal homepage: www.elsevier.com/locate/cnsns



Research paper

Investigation of chaos and memory effects in the Bonhoeffer-van der Pol oscillator with a non-ideal capacitor



Jamieson Brechtl^a, Xie Xie^b, Peter K, Liaw^{b,*}

- ^a The Bredesen Center for Interdisciplinary Research and Education, The University of Tennessee, Knoxville TN 37996, USA
- ^b Department of Materials Science and Engineering, The University of Tennessee, Knoxville, TN 37996, USA

ARTICLE INFO

Article history: Received 5 September 2018 Revised 22 January 2019 Accepted 25 January 2019 Available online 30 January 2019

Keywords: Fractional dynamics Chaos Memory effect Universal dielectric response

ABSTRACT

In this paper, the voltage fluctuations of the Bonhoeffer van der Pol oscillator system with a non-ideal capacitor were investigated. Here, the capacitor was modeled, using a fractional differential equation in which the order of the fractional derivative, α , is also a measure of the memory in the dielectric. The governing fractional differential equation was derived using two methods, namely a differential and integral approach. The former method utilized a hierarchical resistor-capacitor (RC) ladder model while the latter utilized the theory of the universal dielectric-response. It was found that the dynamical behavior of the potential across the capacitor was affected by the parameter α and, therefore, the memory of the system. Additionally, findings indicate that an increase in the memory parameter was associated with an increase in the energy stored in the dielectric. Furthermore, the effects of the dynamical behavior of the voltage on the capacity of the dielectric to store energy was examined. It was found that oscillation death resulted in a higher amount of stored energy in the dielectric over time, as compared to behavior, which displayed relaxation oscillations or chaotic fluctuations. The relatively-lower stored energy resulting from the latter types of dynamical behavior appeared to be a consequence of the memory effect, where the present accumulation of energy in the capacitor is reduced by previous decreases in the potential. Hence, in this type of scenario, the dielectric material can be thought of as "remembering" the past behavior of the voltage, which leads to either a decrease, or an enhancement in the stored energy. Moreover, an increase in the fractional parameter α , under certain conditions, led to the earlier onset of the chaotic voltage oscillations across the capacitor. On the other hand, the corresponding phase portraits showed that the chaotic behavior was heightened, in general, with a decrease in α . The non-ideal capacitor was also found to have a transitory nature, where it behaves more like a resistor as $\alpha \to 0$, and conversely, more like a capacitor as $\alpha \to 1$. Here, a decrease in α was linked to an enhanced metallic character of the dielectric. Finally, a possible link between the complexity of the voltage noise fluctuations and the metallic character of the non-ideal capacitor will be discussed.

© 2019 Elsevier B.V. All rights reserved.

^{*} Corresponding author. E-mail address: pliaw@utk.edu (P.K. Liaw).

1. Introduction

Nonlinear systems are a subject of great importance since they have been observed in a wide range of physical phenomena such as nonlinear mechanics, materials science, and optics [1–7]. One such tool, which is used to study such phenomena, includes the van der Pol (VP) equation, which was introduced by B. van der Pol in his 1920 paper [8]. This type of system can exhibit the chaotic behavior that is characterized by the aperiodic fluctuations, which depends sensitively on the initial conditions [9]. Importantly, this system has played a critical role in the development of nonlinear dynamics.

The Bonhoeffer-van der Pol (BVP) oscillator [10–13] is a modified version of the VP oscillator in which the underlying dynamics of the oscillator are equivalent to a simplified Hodgkin-Huxley model [14,15]. Furthermore, the BVP phenomenon has been examined in chemical systems [16,17], cognitive functioning [18], and neural networks [19]. The BVP scheme has also been considered as a prototype model for excitable systems. Given the right conditions, the BVP system can generate the complicated mixed-mode oscillations (MMOs), which are characterized by alternating large- and small-amplitude excursions in the observed time series [20,21]. Besides the BVP system, MMOs have been observed in chemical and neuronal firing systems [22–25].

As will be discussed later, a major circuit element of the BVP oscillator is a capacitor. In the past, capacitor models that involve a 'universal' dielectric response have been proposed [26,27]. The model was originally based on Curie's empirical law [28], which states that the current produced in a dielectric material exhibits the time-dependent power-law behavior that is proportional to the applied voltage, which is constant. Subsequently, Westerlund et al. expanded upon Curie's model to include a general input voltage, v(t) [26]. At the time, their model contained properties that others did not have, such as the dielectric absorption and insulation resistance.

Interestingly, the capacitor model discussed in [26] utilizes the fractional calculus, which involves derivatives and integrals of arbitrary order [29]. Interestingly, these types of operators involve the integration of the original function multiplied by a power-law function [30]. According to Tarasov, this kind of mathematical operation is also a type of power-like memory function [31]. In the present context, memory means that the present state evolution of a system depends on all past states. Furthermore, long-term memory effects correspond to intrinsic dissipative processes in different physical systems [32,33].

This type of formalism is what led Westerlund to infer that a non-ideal dielectric capacitor will have memory of all earlier voltages. Applying this type of operation to a dielectric capacitor led Westerlund to conclude that these types of materials possess memory effects. Furthermore, he suggested that these memory effects are closely related to the dielectric absorption that occurs during charging [34].

In a circuit whose governing equations consist of non-integer order derivatives (and integrals), the current across the capacitor is proportional to the fractional derivative of the applied potential [35,36]. In terms of the capacitor model, values of α , which denote the order of the derivative, may depend on the type of the dielectric material [26]. For example, in [26,27,37], it was reported that α ranged between 0.6 – 1, where α = 0.6 for SiO_x, while α = \sim 1 for polypropylene.

Besides circuit models, fractional derivatives have been found to be useful in modeling and analyzing various phenomena, such as rheology [38–42], quantum physics [31,43,44], and diffusion [45–47]. Additionally, the non-integer order calculus has other advantages, such as the ability to model complex systems that contain long-range spatial interactions and memory effects [48]. Moreover, the use of the fractional calculus is convenient in modeling circuits since the equations used closely resemble the traditionally applied equations.

Recently, Gafiychuk et al. investigated a BVP system with fractional derivatives of different orders [49]. Here, they studied the system using derivative orders between 0 and 2. It was found that such a system could be less stable than a system involving integer order derivatives. From the results, it was determined that using derivatives with fractional indices make it possible to find new properties for this type of system.

A major goal of the present work, therefore, is to expand upon the results found from the aboveBVP investigations. To accomplish this task, a fractional order BVP model will be investigated to see how inducing memory effects alters its underlying dynamics. Inducing memory into the circuit will be accomplished by exchanging a typical capacitor in the circuit model with a non-ideal one. Another objective of the current investigation will be to examine the interplay between the memory effects and the chaotic behavior of the system. It is believed that this innovative approach will advance our fundamental knowledge on the effects of chaos and memory in the Bonhoeffer van der Pol oscillator system.

2. Modeling and analysis

Fig. 1 shows the circuit diagram of the forced BVP oscillator [50]. The electric circuit consists of an inductor, L, a capacitor, C, a linear resistor, R, a nonlinear negative conductance, G, and two voltage sources, V_0 , and V_1 sin ωt . The nonlinear current, $g(v_c)$, which is a function of the capacitor voltage, v_c , will be expressed as the following cubic polynomial [51]:

$$g(\nu_c) = \beta \nu_c^3 - \gamma \nu_c \; ; \; \beta > 0 \; \gamma \; > 0 \tag{1}$$

The governing equations of the electric circuit, based on Kirchhoff's law, may be represented by the following equations:

$$i_c = C\frac{d\nu_c}{dt} = i - g(\nu_c) \tag{2}$$

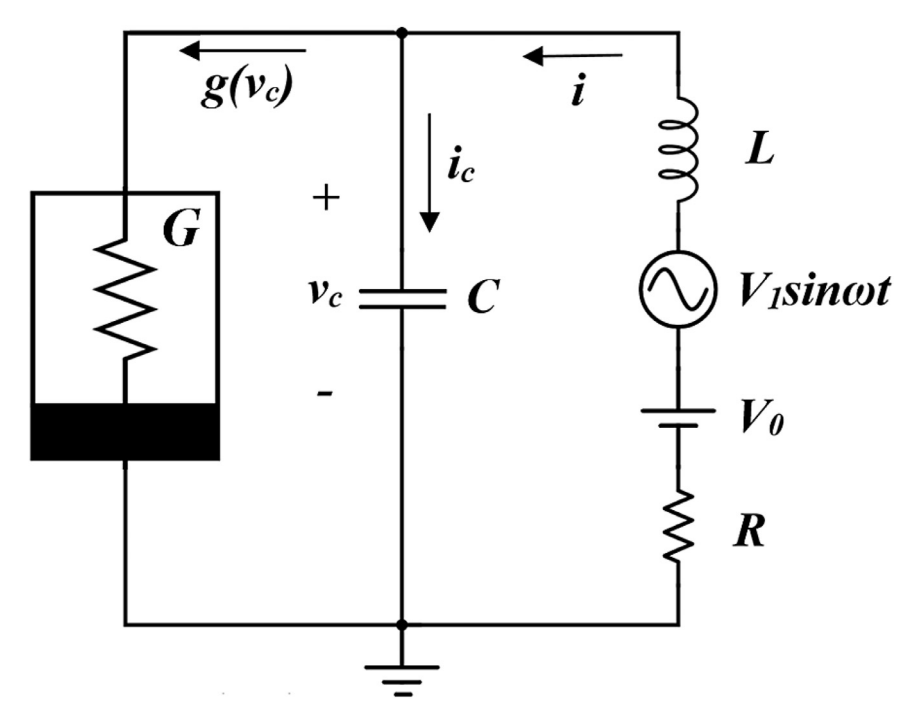


Fig. 1. The circuit diagram for the Bonhoeffer Van der Pol Oscillator system.

$$L\frac{di}{dt} = -v_c - iR + V_0 + V_1 \sin\omega t \tag{3}$$

here, i_c is the current flowing through the capacitor, i is the current arising from the potential source. As was done in [50], we normalize Eqs. (2) and (3) via the following substitutions:

$$\varepsilon = \frac{c}{\gamma^{2}L}, k_{1} = \gamma R, V_{0} = \sqrt{\frac{\gamma}{\beta}} B_{1}, V_{1} = \sqrt{\frac{\gamma}{\beta}} B_{1}, v_{c} = \sqrt{\frac{\gamma}{\beta}} \bar{v}_{c}, i = i = \sqrt{\frac{\gamma^{3}}{\beta}} \bar{i},$$

$$\xi = \frac{t}{\gamma L}, \bar{\omega} = \gamma L \omega, \text{ and } \frac{d}{d\xi} = \gamma L \frac{d}{dt}$$

$$(4)$$

Substituting $\frac{d\tilde{v}_c}{dE}$ in for the normalized capacitor current and expanding $g(v_c)$ give:

$$\frac{d\bar{v}_c}{d\bar{\varepsilon}} = \frac{1}{\varepsilon} \left[\bar{i} - \left(\bar{v}_c^3 - \bar{v}_c \right) \right] \tag{5}$$

$$\frac{d\bar{i}}{d\xi} = -\bar{\nu}_c - k_1\bar{i} + B_0 + B_1\sin\bar{\omega}\xi\tag{6}$$

The parameters, ε , k_1 , and $\bar{\omega}$, were set to 0.1, 0.9, and 1.35, respectively [50]. From here the non-ideal capacitor, in which the current is equal to the fractional order of the applied potential, will be derived in the next couple of sections, using both an integral and a differential method.

2.1. Integral method

In terms of the capacitor, models have been proposed, which considers a 'universal' response of the dielectric material [27]. More specifically, this response is related to the ability of the dielectric system to retain the 'memory' of past excitations. Like the viscoelastic damper, the constitutive relationship between the polarization of the dielectric and a time-varying electric field can be written in terms of the convolution of a response function with the electric field:

$$P(t) = \varepsilon_0 \int_0^\infty f(u)E(t - u)du \tag{7}$$

where P(t) is the time dependent polarization of the dielectric, ε_0 is the dielectric permittivity of the free space, f(u) is the dielectric response function, and E(t) is the electric field between the plates of the capacitor. In addition, taking the Fourier

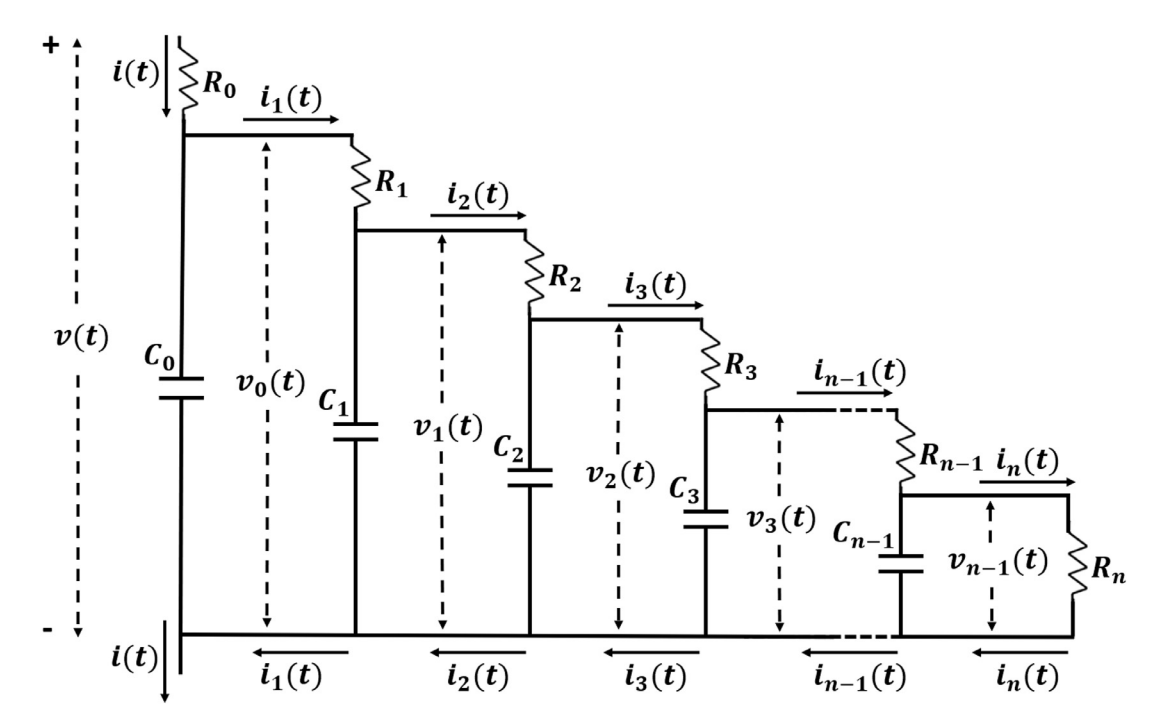


Fig. 2. The RC hierarchical ladder model.

transform of f(u) gives the frequency-dependent susceptibility, $\chi(\omega) = \chi'(\omega) - i\chi''(\omega)$, of the medium. Taking the derivative of the polarization with respect to time yields the current flowing through the capacitor:

$$i_c(t) = \frac{dP}{dt} = \varepsilon_0 \frac{d}{dt} \int_0^\infty f(u)E(t-u)du = \varepsilon_0 \frac{d}{dt} \int_{-\infty}^t f(t-\tau)E(\tau)d\tau \tag{8}$$

where the substitution, $\tau = t - u$, was used. Here we will let $f(t - \tau) = \frac{A}{(t - \tau)^{\alpha}}$ (0 < α < 1), (universal Curie-von Schweidler law [52]) where A is related to ε_0 , the capacitance of the dielectric, and the spacing between the capacitor plates. It should be mentioned that due to its ubiquitous nature, the law can be applied to all types of chemical bonds, all possible types of polarizing species, and to materials containing single crystal, polycrystalline, and amorphous structures [27].

Next, we will assume that at t<0, there is no current flowing through the system and, thus, there is a negligible electric field emanating from the capacitor plate. Furthermore, setting $A=\frac{C_{\alpha}}{\Delta z \varepsilon_{0}}$ and $E(\tau)=\Delta z \upsilon(\tau)$ where C_{α} , Δz and $\upsilon(\tau)$ are respectively the capacitance, the spacing between the plates, and the potential across the capacitor, yields:

$$i_c(t) = C_{\alpha 0} D_t^{\alpha} \nu(t)$$
 (9)

where ${}_{0}D_{t}^{\alpha}\nu(t)$ is the Riemann-Liouville fractional derivative [29] of the potential. Importantly, Eq. (9) was similarly derived by Westerlund et al. [26,34]. It should also be mentioned that C_{α} has units of s^{α}/Ω [34], which arise from fractionally differentiating $\nu(t)$.

2.2. Differential method

In the past, the RC Ladder models have been used to describe the time-dependent current profile in a circuit system [29,53,54]. However, for the present work, a hierarchical model, as proposed by Schiessel et al., will be used [38–40,55]. This type of model is characterized by a tiered structure whose behavior is described by continued fraction expressions. In the past, a similar mathematical framework (as the one shown below) has been used to describe a finite n-section-lumped RC ladder system [56]. Fig. 2 presents the arrangement of the model, which consists of resistor elements on the strut and a capacitor element beneath the resistor. For the modeling and analysis, the following initial conditions will be assumed:

$$i(t \le 0) = i_i(t \le 0) = v(t \le 0) = v_i(t \le 0) = 0 \; ; \; j \in [0, \; n]$$
 (10)

where i_j and v_j are respectively the current and voltage of the jth circuit element (see Fig. 2). Applying Ohm's law to the resistor, R_0 , and capacitor, C_0 , of the circuit model from Fig. 2 yields:

$$\nu(t) = R_0 i(t) + \nu_0(t); \ i(t) = i_1(t) + C_0 \frac{d}{dt} \nu_0(t)$$
(11)

Algebraically manipulating Eq. (11) after applying the Laplace transform and initial condition gives:

$$\frac{\tilde{v}(s)}{R_0\tilde{i}(s)} = 1 + \frac{\frac{1}{R_0C_0}}{s + \frac{\tilde{i}_1(s)}{C_0\tilde{v}_{-0}(s)}}$$
(12)

To generalize Eq. (12), we apply Ohm's law to the kth element in the circuit:

$$v_k(t) = R_{k+1}i_{k+1}(t) + v_{k+1}(t) \; ; \; i_k(t) = i_{k+1}(t) + C_k \frac{d}{dt}v_k(t)$$
 (13)

Applying the Laplace transform to Eq. (13), and using the above method, we can get the following iterative formula:

$$\frac{1}{R_{k+1}} \frac{\tilde{\nu}_k(s)}{\tilde{i}_{k+1}(s)} = 1 + \frac{\frac{1}{R_{k+1}C_{k+1}}}{s + \frac{\tilde{l}_{k+2}(s)}{\tilde{l}_{k+1}\tilde{\nu}_{k+1}(s)}}; \quad k \in [0, n-2]$$
(14)

here, $\tilde{v}(S)$ and $\tilde{i}(s)$ are respectively the Laplace transformed voltage and current. To find the nth term for the ladder model, we plug in k = n - 2 into Eq. (14) with the condition, $\tilde{v}_{n-1}(s) = \tilde{v}_n(s) = R_n \tilde{i}_n(s)$ (based on Fig. 2), which yields:

$$\frac{1}{R_{n-1}} \frac{\tilde{\nu}_{n-2}(s)}{\tilde{i}_{n-1}(s)} = 1 + \frac{\frac{1}{R_{n-1}C_{n-1}}}{s + \frac{1}{R_nC_{n-1}}} \tag{15}$$

Therefore, combining Eqs. (13) - (15), and expanding upon them, gives the following continued fraction form:

$$\frac{\tilde{v}(s)}{R_0\tilde{i}(s)} = 1 + \frac{s^{-1}\left(\frac{1}{R_0C_0}\right)}{1+} \frac{s^{-1}\left(\frac{1}{R_1C_0}\right)}{1+} \frac{s^{-1}\left(\frac{1}{R_1C_1}\right)}{1+} \frac{s^{-1}\left(\frac{1}{R_2C_1}\right)}{1+} \dots \frac{s^{-1}\left(\frac{1}{R_{n-1}C_{n-1}}\right)}{1+} \frac{s^{-1}\left(\frac{1}{R_nC_{n-1}}\right)}{1}$$
(16)

For reasons that will be made obvious, we introduce the continued fraction form for $y(1+y)^{\alpha-1}$ via Eq. (11.7.2) from [57]:

$$y(1+y)^{\alpha-1} = \lim_{n \to \infty} \frac{y}{1+} \frac{(1-\alpha)y}{1+} \prod_{m=3}^{K} \frac{a_m y}{1+}$$
(17)

$$a_{2i} = \frac{i - \alpha}{2(2i - 1)} \ a_{2i + 1} = \frac{i + \alpha - 1}{2(2i - 1)} \tag{18}$$

where $y = s^{-1}(\frac{1}{R_0C_0})$. Writing out the truncated form of Eq. (17) gives:

$$y(1+y)^{\alpha-1} \approx \frac{y}{1+} \frac{(1-\alpha)y}{1+} \frac{\frac{1\cdot(0+\alpha)y}{1\cdot2}}{1+} \frac{\frac{1\cdot(2-\alpha)y}{2\cdot3}y}{1+} \frac{\frac{2\cdot(1+\alpha)y}{3\cdot4}y}{1+} \dots \frac{\frac{n-\alpha}{2\cdot(2n-1)}y}{1}$$
(19)

Setting $\lambda = \frac{1}{R_0 C_0}$ and comparing term-by-term Eqs. (16) and (19) yield:

$$\frac{1}{R_1C_0} = (1-\alpha)\lambda; \ \frac{1}{R_1C_1} = \frac{\alpha}{2}\lambda; ...; \ \frac{1}{R_{n-1}C_{n-1}} = \ \frac{n+\alpha-2}{2(2n-3)}\lambda; \ \frac{1}{R_nC_{n-1}} = \frac{n-\alpha}{2(2n-1)}\lambda$$
 (20)

From the above equations, each C_k and R_k may be written in terms of their respective C_0 , R_0 as [38]:

$$R_k = (2k - 1)\frac{\Gamma(1 - \alpha)}{\Gamma(\alpha)} \frac{\Gamma(k + \alpha - 1)}{\Gamma(k - \alpha + 1)} R_0 \tag{21}$$

$$C_k = 2\frac{\Gamma(\alpha)}{\Gamma(1-\alpha)} \frac{\Gamma(k-\alpha+1)}{\Gamma(k+\alpha)} C_0 \tag{22}$$

where Γ is the gamma function. If we substitute the terms from Eq. (20) into Eq. (16) and take the limit $n \to \infty$, we obtain:

$$\frac{\tilde{v}(s)}{R_0\tilde{i}(s)} = 1 + \left(\frac{\lambda}{s}\right) \left(1 + \frac{\lambda}{s}\right)^{\alpha - 1} \tag{23}$$

Under the right conditions, Eq. (23) may be written as:

$$\frac{\tilde{\nu}(s)}{R_0\tilde{i}(s)} = \left(\frac{\lambda}{s}\right)^{\alpha} = \left(\frac{1}{R_0C_0s}\right)^{\alpha} \tag{24}$$

which is valid for $6R_0C_0 \le 1/s \le \frac{1}{6}R_0C_0n^2$ [29]. Now, taking the inverse Laplace transform of Eq. (24) in this range yields:

$$i(t) = R_0^{\alpha - 1} C_0^{\alpha} D_t^{\alpha} v(t) \; ; \; 6R_0 C_0 \; \le \; t \; \le \; \frac{1}{6} R_0 C_0 n^2$$
 (25)

Importantly, the relation from the Eq. (25) is preserved for long times if there are a sufficiently large number of ladder elements in the capacitor. If we are dealing with a dielectric material that exhibits a loss peak in certain frequency ranges, a further restriction must be applied:

$$6R_0C_0 \le t < \frac{1}{\omega_p} \tag{26}$$

where ω_p is the frequency at which the peak occurs. Therefore, if a loss peak is observed, the condition imposed by Eq. (26) is necessary for the application of the Curie-von Schweidler law [i.e., $f(t) \propto t^{-\alpha}$] to Eq. (8). To increase the reduced time range imposed by the large peak frequencies, one can select sufficiently small-valued resistors and capacitors. As discussed in [38], R_k and C_k may be chosen in such a way that $R_0 = R$ and $C_0 = C$. In doing so, we obtain:

$$i_c(t) = R^{\alpha - 1} C^{\alpha}_{0} D_c^{\alpha} \nu_c(t) \tag{27}$$

Notice the similarities between the above equation and Eq. (9). In fact, they only differ in their coefficients, where the former has a coefficient defined as C_{α} , while the latter is given by $R^{\alpha-1}C^{\alpha}$. As observed in Eq. (27), when $\alpha=1$, the circuit element behaves as a standard capacitor, while for $\alpha=0$, the device behaves purely as a resistor [26,34]. Therefore, a dielectric capacitor in this context can be thought of as one that behaves in a fashion that is intermediate between those of a standard capacitor and a resistor.

In terms of the behavior of the above model, the following may explain its underlying dynamics. As a voltage, $\theta_0 v(t)$ (θ_0 is the Heaviside step function), is suddenly applied to the capacitor system (see Fig. 2), the potential is initially only experienced by the first resistor, R_0 . Here, the element, R_0 , in addition to the other R_i 's, may represent some resistive or energy-loss mechanism. After a brief period, the voltage on the first capacitor, C_0 , begins to rise, which represents the storage of energy in the structure. Simultaneously, the current flows across the next resistor, R_1 , creating a potential across the element. In this way, the voltage propagates continuously down the ladder, inducing the energy transfer along the way. Almeida et al. put forth the following approximation for the fractional derivative of a time dependent function, x(t) [58]:

$$a D_t^{\alpha} x(t) \approx A(N,\alpha)(t-a)^{-\alpha} x(t) + B(N,\alpha)(t-a)^{1-\alpha} \dot{x}(t) - \sum_{p=2}^{N} C(p,\alpha)(t-a)^{1-p-\alpha} V_p(t) = \phi(t,x,\dot{x})$$
 (28)

where $0 < \alpha < 1$. Additionally, $A(N, \alpha)$, $B(N, \alpha)$, $C(p, \alpha)$, and $V_p(t)$ are defined as the following:

$$A(N,\alpha) = \frac{1}{\Gamma(1-\alpha)} \left[1 + \sum_{p=2}^{N} \frac{\Gamma(p-1+\alpha)}{\Gamma(\alpha)(p-1)!} \right]$$
 (29)

$$B(N,\alpha) = \frac{1}{\Gamma(2-\alpha)} \left[1 + \sum_{p=1}^{N} \frac{\Gamma(p-1+\alpha)}{\Gamma(\alpha-1)p!} \right]$$
(30)

$$C(p,\alpha) = \frac{1}{\Gamma(2-\alpha)\Gamma(\alpha-1)} \frac{\Gamma(p-1+\alpha)}{(p-1)!}$$
(31)

$$V_p(t) = (1 - p) \int_a^t (\tau - a)^{p - 2} x(\tau) d\tau \; ; \; p \in [2, N] \; p \in \mathbb{N}$$
 (32)

The moments, V_p , are regarded as solutions to the following system of differential equations:

$$\dot{V}_p(t) = (1 - p)(t - a)^{p-2}x(t) \tag{33}$$

$$V_p(a) = 0, \ \forall p \in [2, N]$$
 (34)

The power of Eqs. (28)–(34) lies in their ability to approximate the fractional derivative, using the original function and its first order derivative. With regards to Eq. (28), a was set to 0 and t was chosen sufficiently small as to avoid singularities and complex values. Now, plugging in $\frac{d^{\alpha}}{dE^{\alpha}}\bar{\nu}_{c}(\xi)$ for the normalized capacitor current in Eq. (5) gives:

$$\frac{d^{\alpha}\bar{\nu}_{c}}{d\xi^{\alpha}} = \frac{1}{\varepsilon} \left[\bar{i} - \left(\bar{\nu}_{c}^{3} - \bar{\nu}_{c} \right) \right] \tag{35}$$

$$\frac{d\bar{i}}{d\xi} = -\bar{\nu}_c - k_1 \bar{i} + B_0 + B_1 \sin\bar{\omega}\xi \tag{36}$$

Using Eq. (28), we may approximate $\frac{d\bar{v}_c}{d\bar{\varepsilon}}$, which yields:

$$\frac{d\bar{v}_c}{d\xi} \approx \varphi(\xi) \left\{ \frac{1}{\varepsilon} \left[\bar{i}(\xi) - \bar{v}_c^3(\xi) + m_1(\xi)\bar{v}_c(\xi) \right] + m_2(\xi) \right\}$$
(37)

$$m_1(\xi) = 1 - A(\alpha, N)(\xi - a)^{-\alpha}$$
 (38)

$$m_2(\xi) = \sum_{p=2}^{N} C(p,\alpha)(\xi - a)^{1-p-\alpha} V_p(\xi)$$
(39)

$$\varphi(\xi) = \frac{1}{B(\alpha, N)} (\xi - a)^{\alpha - 1} \tag{40}$$

One can notice with Eqs. (38)–(40) that in the limit of $\alpha \to 1$, $m_1(\xi) = 1$, $m_2(\xi) = 0$ while $\varphi(\xi) = 1$, and Eq. (37) converts to the case for the ordinary derivative. One can now handily solve for the potential, $\bar{\nu}_c$, and the current, \bar{i}_c using conventional numerical techniques. For the present work, the system was solved by means of the fourth-order Runge-Kutta method, using a time step of $2\pi/1024\bar{\omega}$ [50]. Additionally, the initial condition of $i_c(0) = v_c(0) = 0$ will be used for this system.

2.2.1. Error analysis

To examine the accuracy of the differential model, the following error formula was used [58,59]:

$$E[x(t), \tilde{x}(t)] = \sqrt{\int_a^b \left[x(t) - \tilde{x}(t)\right]^2 dt}$$
(41)

where E is the error approximation, and x(t), $\tilde{x}(t)$ are respectively the analytical and approximated solution to the fractional differential equation. As was done in [60], the limits of the integral for Eq. (41) were set to $a = \sim 0$ and b = 1. The error analysis was applied to the following type of fractional differential equation:

$${}_{0}D_{t}^{\alpha}x(t) + x(t) = F(t) + G(t) \tag{42}$$

here, $\alpha \in (0,1)$, and F(t), G(t) are functions of t. With regards to this work, the method was applied to the following set of equations:

$$\int_{0}^{0.5} D_t^{0.5} + \chi(t) = t^{0.5} E_{1,1.5}(-t) + e^{-t}$$
(43a)

$${}_{0}D_{t}^{0.5}x(t) + x(t) = \sin(\pi t) + \pi t^{0.5}E_{2,1.5}[-(\pi t)^{2}]$$
(43b)

$$\begin{cases}
 {0}D{t}^{0.5} + x(t) = t^{0.5}E_{1,1.5}(-t) + e^{-t} \\
 {0}D{t}^{0.5}x(t) + x(t) = \sin(\pi t) + \pi t^{0.5}E_{2,1.5}[-(\pi t)^{2}] \\
 {0}D{t}^{0.5}x(t) + x(t) = t^{4} + \frac{\Gamma(5)}{\Gamma(4.5)}t^{3.5}
\end{cases} (43a)$$

Conventional analytical methods can be applied to Eqs. 43(a)–(c), which give respective solutions of $t^{0.5}E_{1.1.5}(-t)$ (two parameter Mittag-Leffler function [30]), $\sin(\pi t)$, and t^4 . The approximate solutions for Eqs. (43a) and (43c), as found using Eqs. (28)-(34), were then plotted alongside its analytical solution in Fig. 3(a)-(c). As can be seen, the error ranged from 0.001 for Eq. (43a) to a maximum of 0.072 for Eq. (43c). The error values associated with these equations were also found to be comparable to results discussed in [59].

2.3. Chaos detection algorithm

Cafagna et al. [61] proposed an algorithm to determine if a given dynamical system is chaotic. Importantly, this method can be applied directly to the time series data instead of requiring phase space reconstruction, as was used with previous algorithms [61]. More recently, this model was extended to include fractional-ordered systems [62,63]. For the analysis, one takes a given discrete set of data $\phi(n)$ obtained from the underlying dynamics. From the data set, one defines the following equation:

$$p(n) = \sum_{j=1}^{n} \phi(j) \cos[\theta(j)] \quad n = 1, 2, 3 \dots$$
 (44)

where:

$$\theta(j) = jc + \sum_{i=1}^{j} \phi(j) \quad j = 1, 2, 3 \dots n$$
 (45)

and $c \in \mathbb{R}^+$ is a constant that is chosen at random [63]. Next, define the mean square displacement for a finite set of data:

$$M(n) = \frac{1}{N-n} \sum_{j=1}^{N-n} \left[p(j+n) - p(j) \right]^2 \qquad 1 \le n \le N$$
 (46)

Now define the asymptotic growth rate of the mean square displacement [61]:

$$K = \lim_{n \to \infty} \frac{\log[M(n)]}{\log(n)} \tag{47}$$

From the results, a K value relatively close to zero indicates that the dynamics is regular while K relatively close to 1 signifies chaotic behavior.

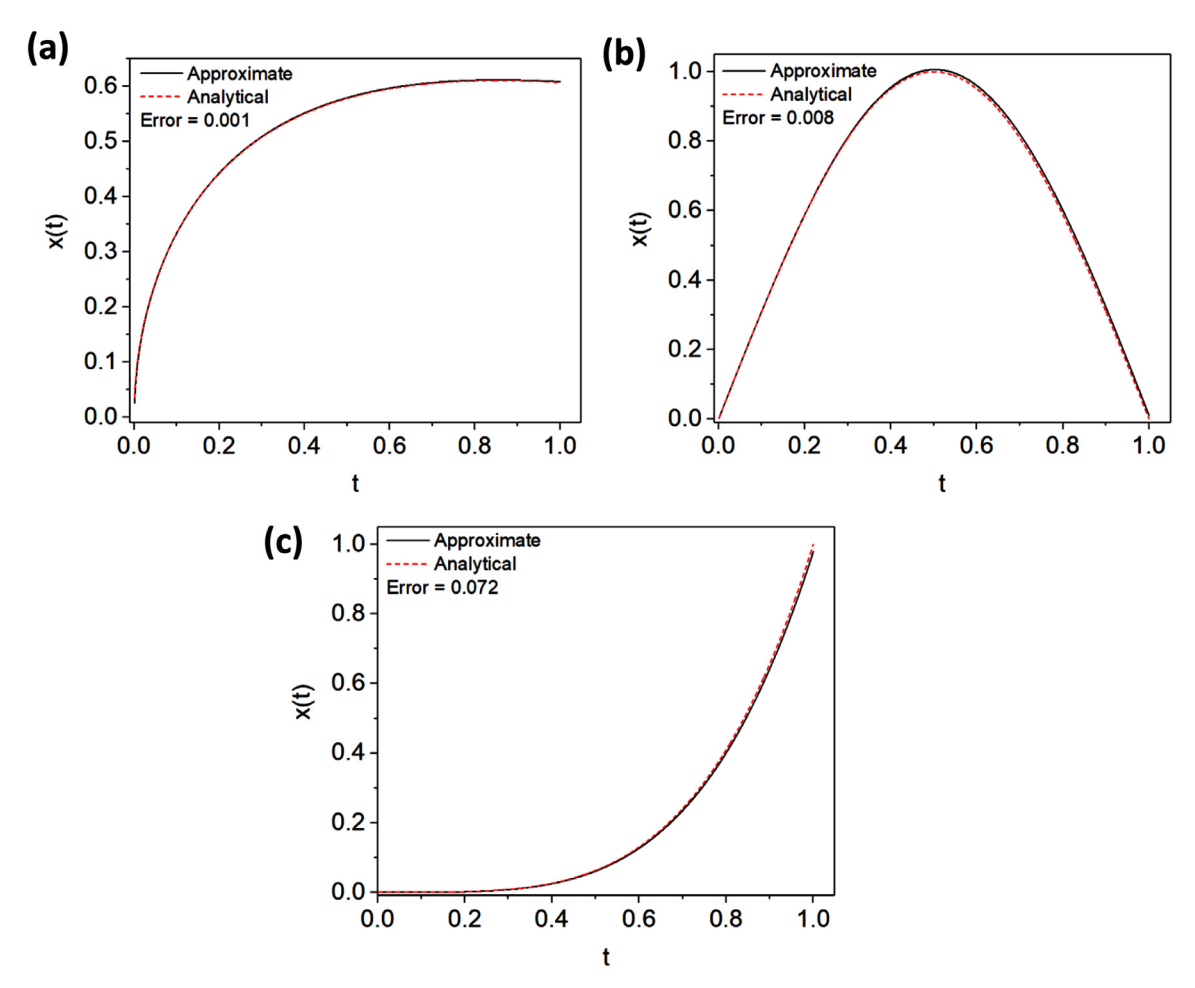


Fig. 3. Analytic versus approximation for the solutions of the differential equation (a) $(43a) x(t) = t^{0.5} E_{1.1.5}(-t)$, (b) $(43b) x(t) = \sin(\pi t)$, and (c) $(43c) x(t) = t^4$. (For the interpretation of the references to color in this figure legend, the reader is referred to the web version of this article.)

3. Results

The one-parameter bifurcation diagram, according to the model for the integer-order derivative (α = 1), was solved for B_0 = 0.21 in a similar manner as that in [50]. The results, which can be seen in Fig. 4(a), agree with the results presented in the above work. Based on the figure, the fluctuations exhibit the chaotic behavior in the regions of 0 < B_1 < 2.8 × 10⁻³ and 3.5 × 10⁻² < B_1 < 5.6 × 10⁻². On the other hand, periodic doubling can be observed for 5.6 × 10⁻² < B_1 < 6.4 × 10⁻². Furthermore, there are period halving bifurcations at B_1 = 0.063, 0.056, 0049. In the other regions of the graph, there are only one-point attractors.

To compare the results for the integer-order derivative with the fractional-order derivative model, the one-parameter bifurcation diagram, for the case of $\alpha = 0.6$ and $B_0 = 0.21$ was plotted in Fig. 4(b). As can be observed, the voltage behavior wassignificantly different as compared to the behavior observed in Fig. 4(a). For instance, there was no observed chaotic behavior in the entire region. Curiously, the voltage exhibited discontinuities at $B_1 = 0.041$, 0.043, and 0.045. This result suggests that the bifurcation diagram is affected by changes in the order of the fractional derivative, and hence the memory of the system.

Fig. 5 shows the potential, $\bar{\nu}_c(\xi)$, for $B_1 = 0.0065$ with $0 \le \xi \le 60$ and $0.6 \le \alpha \le 1$. As can be seen, the magnitude of the oscillations decreases with increasing ξ , eventually leading to the oscillation death. Furthermore, the amplitude of the oscillations, in general, decreases with respect to α . Moreover, the amplitude of the fluctuations appears to begin dampening at earlier times as α is decreased. Fig. 6 displays the asymptotic growth rate, K, as a function of the data index value for the dynamical data corresponding to Fig. 5. As can be seen, the curves for each condition are relatively close to zero, implying that the potential does not exhibit chaotic behavior for the given parameters.

The potential, $\bar{v}_c(\xi)$, for $B_1 = 0.0415$, where the oscillator exhibits the chaotic behavior for $\alpha = 1$ (see Fig. 7), was plotted for $0 \le \xi \le 100$ and $0.6 < \alpha < 1$. For $\alpha = 1$, the chaotic behavior can be observed throughout the given interval, whereas the same behavior is only displayed for earlier times when α is equal to 0.6, 0.8, and 0.9. Furthermore, for the same α values,

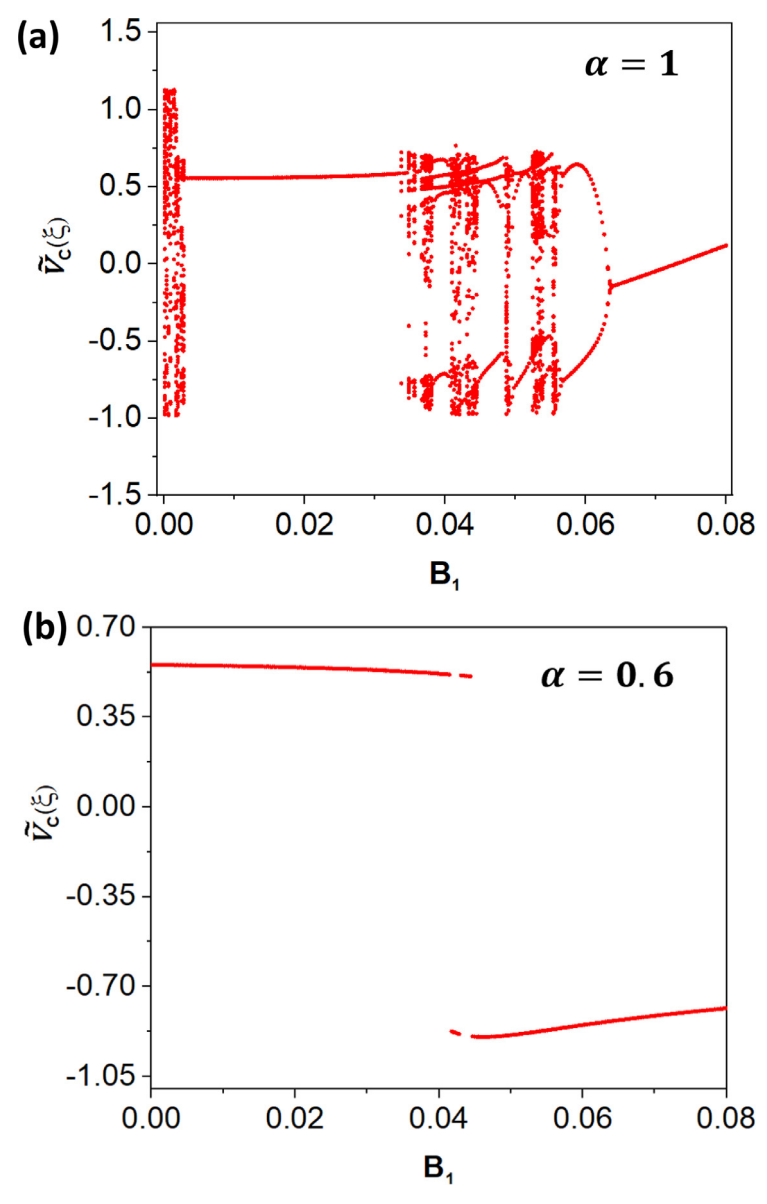


Fig. 4. The one-parameter bifurcation diagram for the potential oscillations for the case of (a) $\alpha = 1$, and (b) $\alpha = 0.6$ for B_1 ranging from 0 to 0.08, and $B_0 = 0.21$. (For the interpretation of the references to color in this figure legend, the reader is referred to the web version of this article.)

the oscillations appear to settle into the relaxation oscillations after the period of transient chaos. Interestingly, for $\alpha = 0.7$, the fluctuations exhibit the oscillation death. Fig. 8 displays the asymptotic growth rate as a function of the data index value N for the dynamical data corresponding to Fig. 7. For $\alpha = 0.7$, K was close to zero, implying that the underlying dynamics were not chaotic. On the other hand, the growth rate corresponding to α values equal to 0.6, 0.8, 0.9, and 1 were relatively close to 1, which implies that their behavior was chaotic in nature. Furthermore, K attained the highest values for $\alpha = 0.8$.

The power, P(t), into the capacitor is simply the product of the current and the voltage across the element. To write the power as a function of time, the normalized potential, current, and variable ξ , were converted back into their original form, as found in Eq. (2). The above was done by setting the inductance L, γ , and β to 1 Vs/A, 1 A/V, and 1 A/V³, respectively. Using these definitions, P(t) can be written as:

$$P(t) = \begin{cases} C_{\alpha} v_c(t)_0 D_t^{\alpha} v_c(t) & 0 < \alpha < 1 \\ C_{\alpha} v_c(t) i_c(t) & \alpha = 1 \end{cases}$$

$$\tag{48a}$$

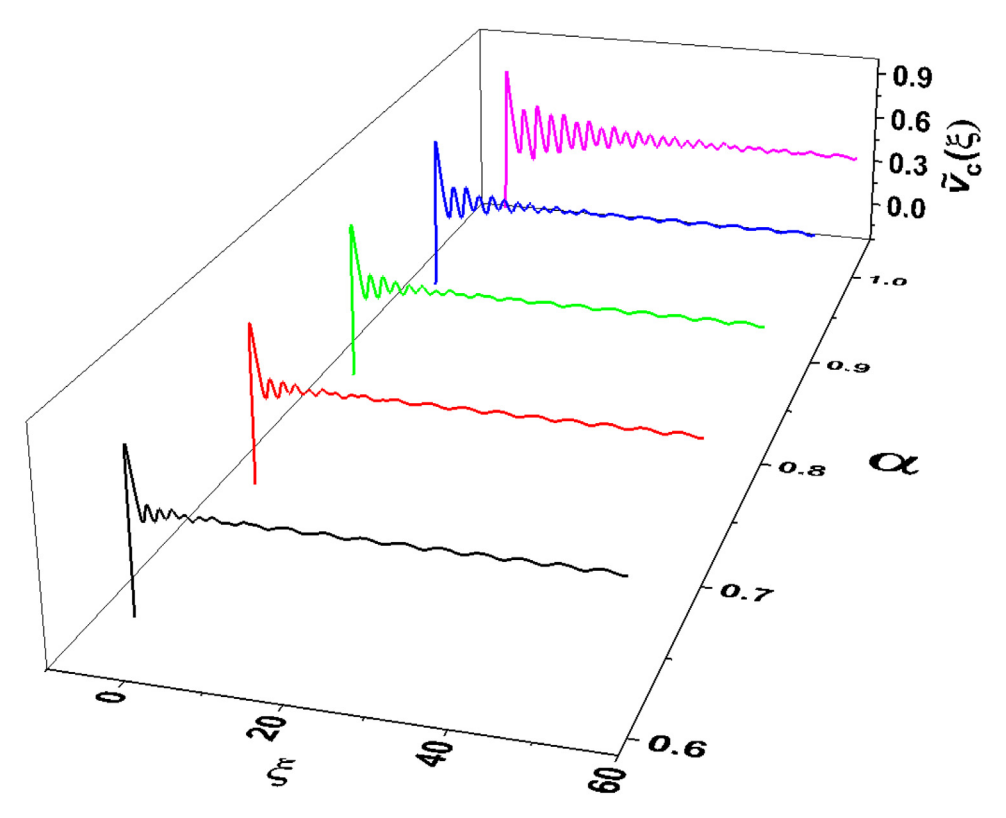


Fig. 5. The potential $\bar{v}_c(\xi)$ for $0 < \xi < 60$, $0.6 < \alpha < 1$, and $B_1 = 0.0065$. (For the interpretation of the references to color in this figure legend, the reader is referred to the web version of this article.)

Using the relation $i_c(t) = \frac{d}{dt}v_c(t)$ (for $\alpha = 1$) and integrating the power gives the energy, W(t), of the capacitor:

$$W(t) = \begin{cases} \frac{C_{\alpha}}{\Gamma(1-\alpha)} \int_{0}^{t} v_{c}(t') \left[\int_{0}^{t'} \frac{\dot{v}z_{c}(\tau)}{(t'-\tau)^{\alpha}} d\tau + \frac{v_{c}(0)}{t'^{\alpha}} \right] dt' & 0 < \alpha < 1 \\ \frac{1}{2} C_{\alpha} v_{c}^{2}(t) & \alpha = 1 \end{cases}$$
(49a)

It should also be mentioned that for Eq. (49a), the Caputo definition of the fractional derivative was used [64]. For our case, the second term, $\frac{v_c(0)}{t'^{\alpha}}$, vanishes due to the initial condition, $v_c(0) = 0$. However, if the potential is a constant non-zero value $[v_c(0) \neq 0]$, the energy stored in this type of the capacitor will be proportional to $t^{1-\alpha}$. This result has been derived in the previous work involving fractional-order capacitors [65].

Based on Eq. (49a), the energy stored in the non-ideal capacitor is equal to the integral of the applied voltage multiplied by a current that has inherent memory effects. Furthermore, setting $C_{\alpha} = \frac{\Gamma(1-\alpha)}{R^{\alpha-1}C^{\alpha}}$ for the coefficient from Eq. (49a) and taking the limit as $\alpha \to 0$, one recovers the energy across a standard resistor. The above statement supports the idea that the non-ideal capacitor is a circuit element, which is transitory between a capacitor and a resistor.

To calculate the energy stored on the capacitor, the coefficient, C_{α} , as proposed by Westerlund et al. [26], will be used:

$$C_{\alpha} = \begin{cases} \varepsilon_{0} \varepsilon_{r} \omega^{1-\alpha} \sin\left(\frac{\pi \alpha}{2}\right) \frac{A}{d} & 0 < \alpha < 1\\ \varepsilon_{0} \varepsilon_{r} \frac{A}{d} & \alpha = 1 \end{cases}$$
 (50a)

Here ω is the angular frequency of the harmonically-varying field, ε_0 is the permittivity of the free space with a value of 8.854×10⁻¹² As/Vm, ε_r is the relative permittivity of the dielectric, A is the area of the capacitor plates, and d is the distance between them. Notice how Eq. (50a) converts to Eq. (50b) for $\alpha = 1$. To keep in line with the parameters used for this study, ω was chosen to be 1.35 Hz.

The values, ε_r , were found in the literature for various substances that corresponded to similar α values as those used in the present work. More specifically, the materials were polypropylene ($\alpha=1$, $\varepsilon_r=2.2$), stearic acid ($\alpha=0.95$, $\varepsilon_r=2.59$), anthracene ($\alpha=0.85$, $\varepsilon_r=3$), and silicone dioxide ($\alpha=0.6-0.7$, $\varepsilon_r=3.9$) [26,27,66-68]. To match the results of the current work, the fractional parameter was rounded down to 0.9, 0.8, and 0.6, for the stearic acid, anthracene, and silicone dioxide, respectively. Since ε_r was not available for $\alpha=0.7$, it was estimated by interpolating the values above, giving approximately 3.45 for the permittivity. From the listed values, it is evident that the fractional exponent decreases with respect to this parameter.

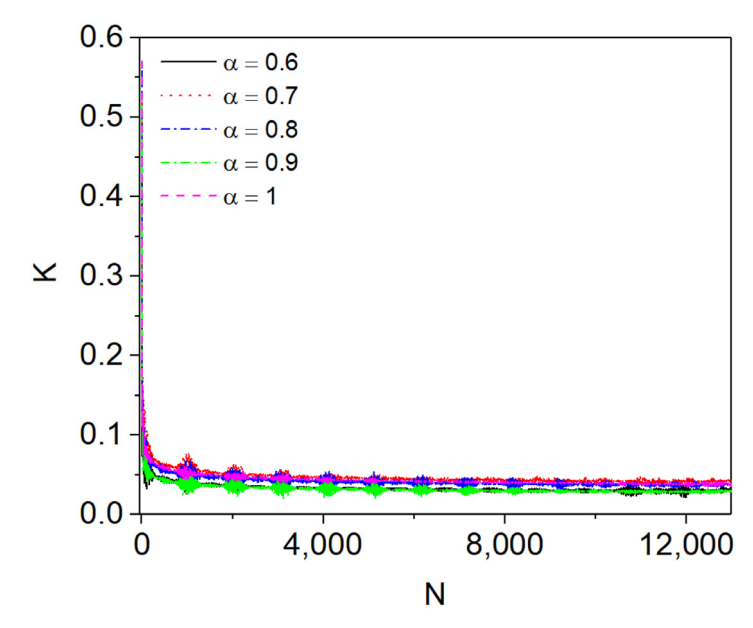


Fig. 6. Plot of K versus the length of the time series N for $0.6 < \alpha < 1$, and $B_1 = 0.0065$. (For the interpretation of the references to color in this figure legend, the reader is referred to the web version of this article.)

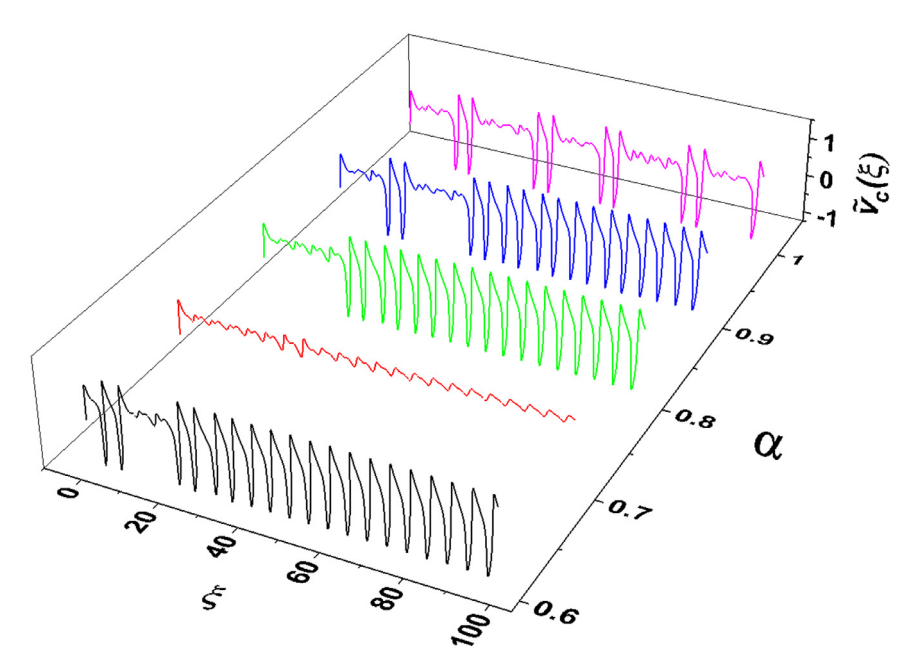


Fig. 7. The potential, $\bar{v}_c(\xi)$, for $0 < \xi < 100$, $0.6 < \alpha < 1$, and $B_1 = 0.0415$. (For the interpretation of the references to color in this figure legend, the reader is referred to the web version of this article.)

Fig. 9 presents the energy stored on the capacitor as a function of t for $0.6 \le \alpha \le 1$ with $B_1 = 0.0065$. Here the capacitor was assumed to have a volume of 1 cm³ (d = 1 cm, A = 1 cm²). As can be seen in the graph, the energy increases in a monotonic fashion with respect to t for $0.6 \le \alpha \le 0.9$. In addition, the curves decrease with respect to α .

Fig. 10 shows the energy stored on the capacitor for B_1 = 0.0415. Unlike Fig. 9 (for B_1 = 0.0065), the energy exhibited observable fluctuations for α < 1. However, like Fig. 9, W(t) was larger for α < 1. On the other hand, the energy associated with α = 0.7, where there was the oscillation death, attained higher values for t > \sim 4 s. Like the potential values, the energy for the same α displayed the smallest oscillations, as compared to the other exponents.

Fig. 11 presents the one-parameter bifurcation diagrams for B_1 ranging from 0 to 0.08 as a function of the fractional exponent, α . It should also be stated that the points for $\alpha = 1$, at a given B_1 value, correspond to the $\bar{\nu}_c(\xi)$ values that can be observed in Fig. 1. When $B_1 = 0$, the potential tends to reach a single value of \sim 0.555 until $\alpha = 0.99$, where the

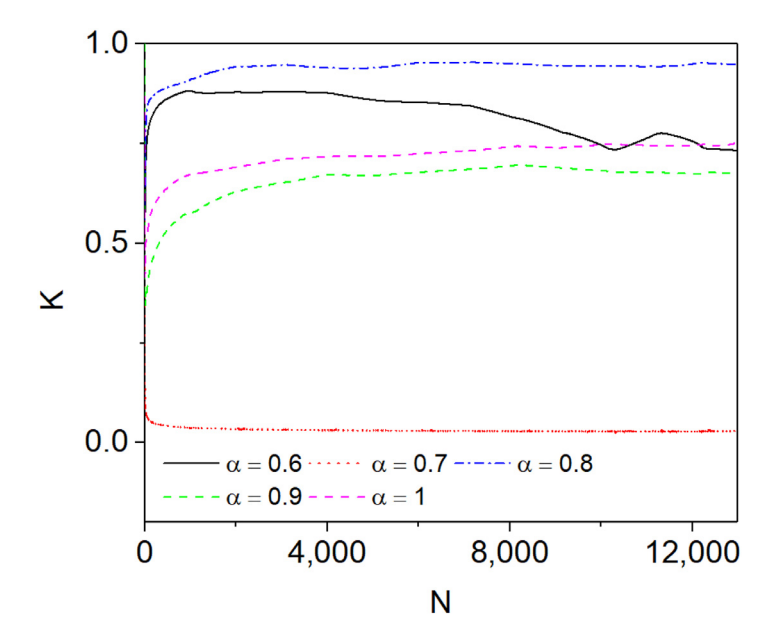


Fig. 8. Plot of *K* versus the length of the time series N for $0.6 < \alpha < 1$, and $B_1 = 0.415$. (For the interpretation of the references to color in this figure legend, the reader is referred to the web version of this article.)

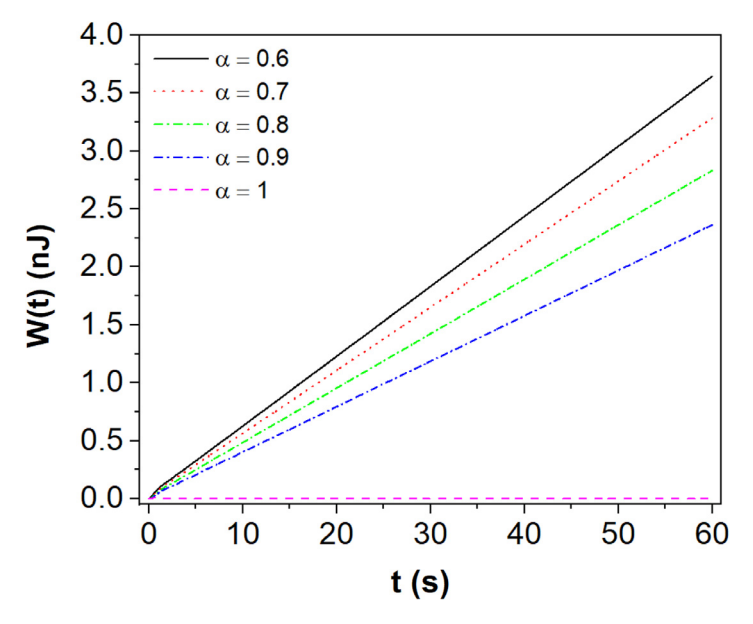


Fig. 9. The energy stored on the capacitor, W(t), for $0 \le t \le 60$, $0.6 < \alpha < 1$, and $B_1 = 0.0065$. (For the interpretation of the references to color in this figure legend, the reader is referred to the web version of this article.)

chaotic behavior emerges. For B_1 ranging from 0.01 to 0.03, the curve does not exhibit the chaotic behavior for the range of fractional exponents. For B_1 = 0.02, there is a saddle node bifurcation centered at α = 0.96, whereas for B_1 = 0.03, a saddle node is centered around 0.97. For B_1 = 0.04, a bifurcation occurs at α ~ 0.955, and there is also erratic behavior for α = 0.83, which is followed by a drop in $\bar{\nu}_c(\xi)$ at α = 0.84. Moreover, the region of the chaotic behavior near α = 0.83, as exhibited for B_1 = 0.04, increases in size as B_1 increases. With respect to B_1 = 0.04, period doubling bifurcations were observed at α = 0.96, 0.965, and 0.97 in the corresponding graph. For B_1 = 0.05, period doubling bifurcations were observed at α = 0.97, 0.98, and 0.99. Furthermore, there is a saddle node bifurcation centered at 0.0865. For B_1 = 0.06, there was one apparent period doubling bifurcation at α = 0.99, whereas there was a saddle node bifurcation centered at 0.84. Likewise for B_1 = 0.07 and 0.08, there were saddle node bifurcations centered at 0.83 and 0.82, respectively.

To examine the interplay between the memory effects and chaotic behavior of the potential in the non-ideal capacitor, $\bar{\nu}_c(\xi)$ was plotted for ξ values ranging from 150 to 1400 with $B_1 = 0.06$ and α ranging from 0.6 to 0.9, as shown in Fig. 12.

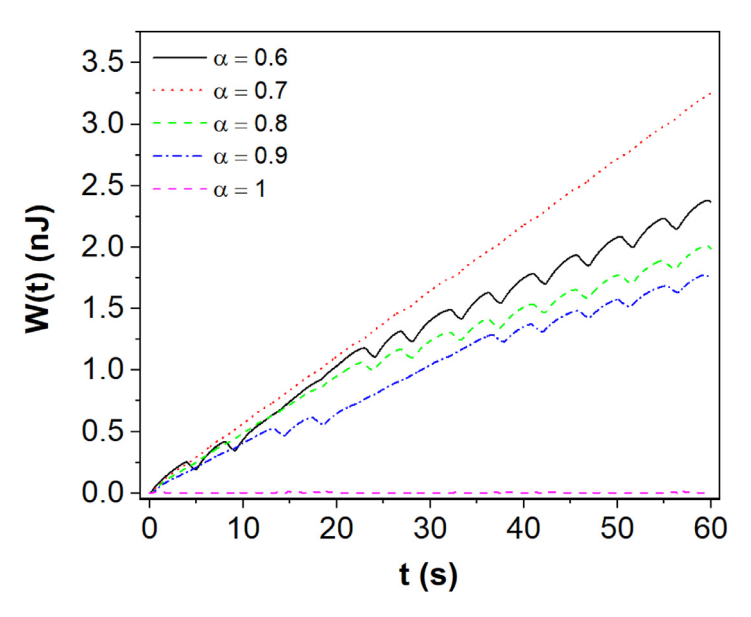


Fig. 10. The energy stored on the capacitor, W(t), for $0 \le t \le 60$, $0.6 < \alpha < 1$, and $B_1 = 0.0415$. (For the interpretation of the references to color in this figure legend, the reader is referred to the web version of this article.)

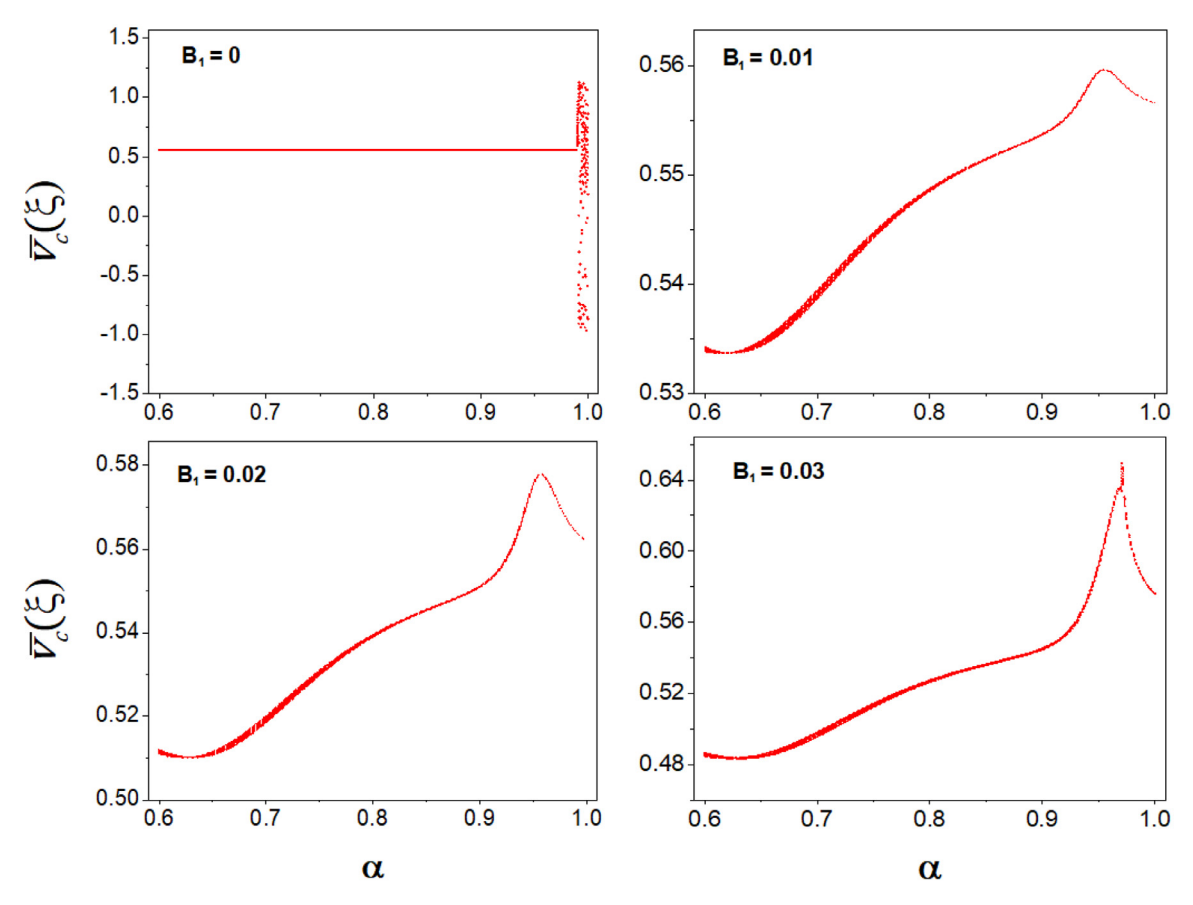
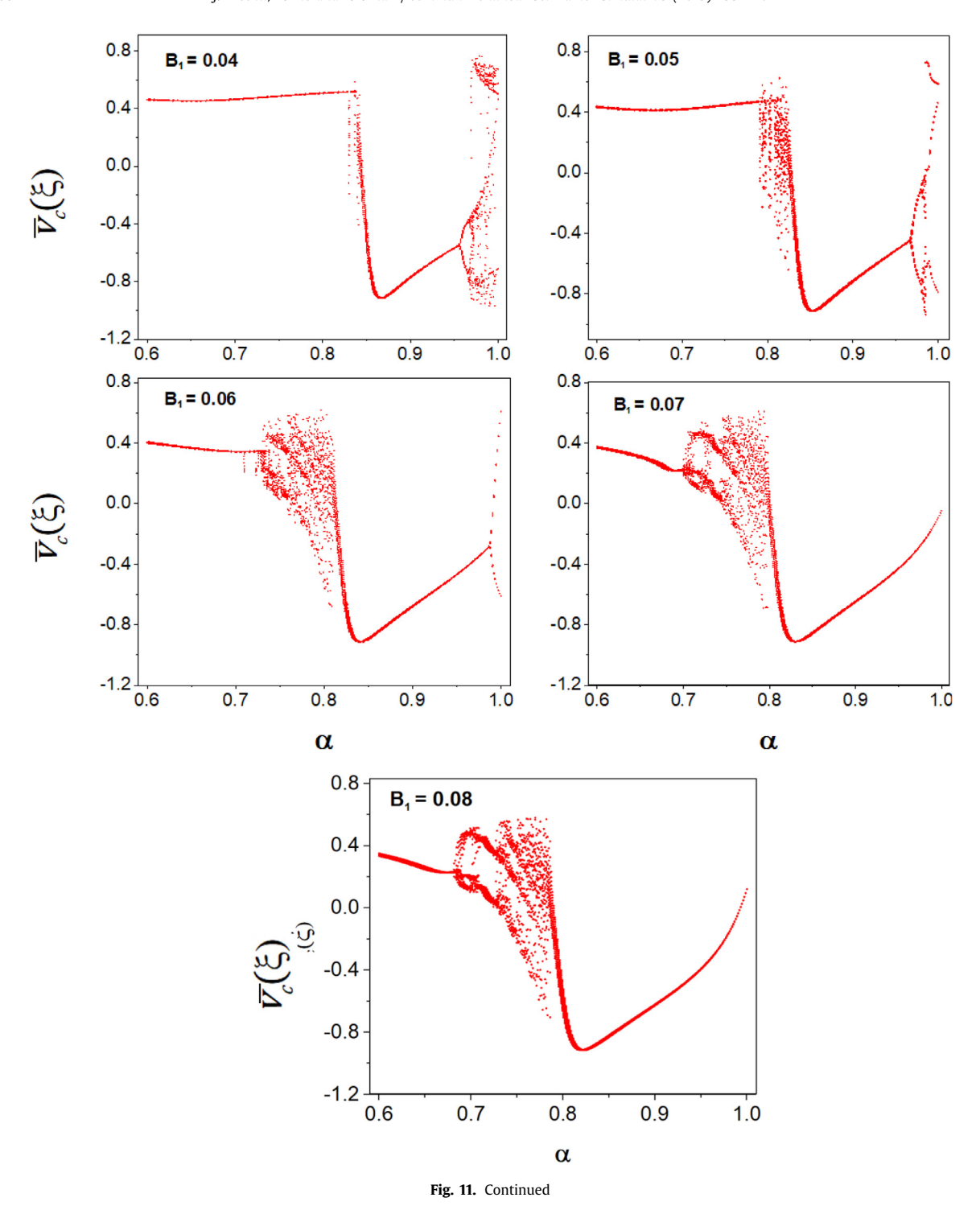


Fig. 11. The one-parameter bifurcation diagram for the potential oscillations corresponding to $0.6 < \alpha < 1$ and B_1 ranging from 0 to 0.08. (For the interpretation of the references to color in this figure legend, the reader is referred to the web version of this article.)



To give a more detailed picture of the chaotic and non-chaotic behavior of the above figure, a magnification of the important regions is displayed in Fig. 13. As can be seen in the figures, the time until the onset of chaos increases, as α is increased. Additionally, the fluctuations are quasiperiodic for $\alpha = 0.9$ in the given interval. Furthermore, the relaxation oscillations (for $\alpha \leq 0.7$) that occur after the chaotic behavior are smaller in magnitude, as compared to the fluctuations beforehand.

The corresponding phase planes for the results from Fig. 11 can be observed in Fig. 14. For each graph, the current, $i(\xi)$, was plotted with respect to $v_c(\xi)$. As can be seen, the curves for $\alpha < 0.9$ possess unstable limit cycles [20] that are indicative of the chaotic behavior. Moreover, the size of the attractor region is maximized for $\alpha = 0.7$, indicating that the

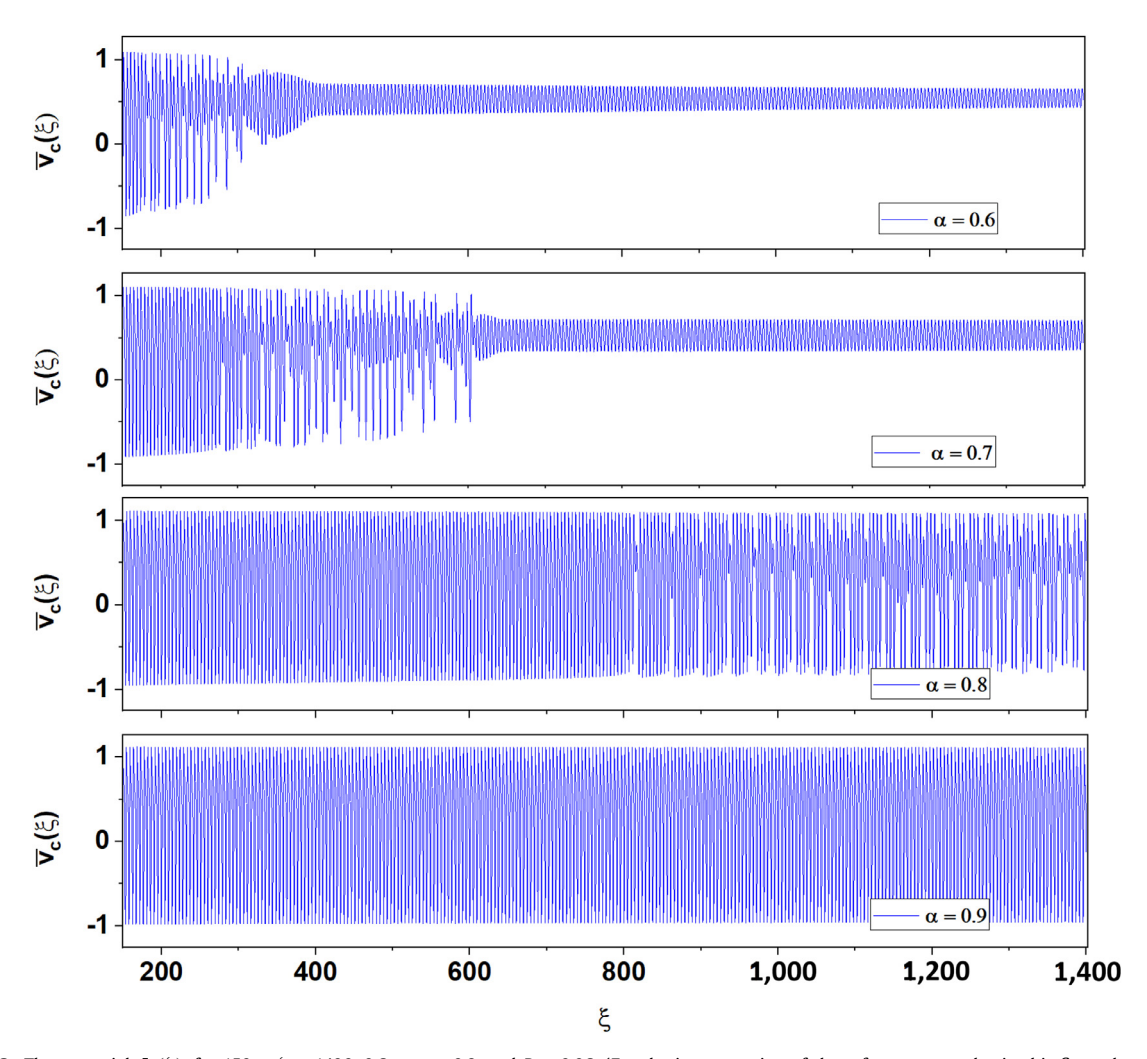


Fig. 12. The potential, $\bar{\nu}_c(\xi)$, for 150 $\leq \xi \leq$ 1400, 0.6 $< \alpha <$ 0.9, and $B_1 =$ 0.06. (For the interpretation of the references to color in this figure legend, the reader is referred to the web version of this article.)

oscillations are more irregular, as compared to the other conditions in the given domain. In contrast, the fluctuations for $\alpha = 0.9$ are quasiperiodic in which the behavior is signified by a phase portrait that contains a stable limit cycle.

To gain a better understanding of how the current moves down the ladder system, the ratios R_k/R_0 and C_k/C_0 elements were calculated, using Eqs. (21) and (22), and are displayed in Figs. 15 and 16 for k=1–20. As can be observed in the graphs, the values appear to increase or decrease in a monotonic fashion. Interestingly, the resistor values appear to behave in an opposite manner, as compared to the capacitor elements. It can be seen from Fig. 15 that for $0.6 < \alpha < 0.9$, R_k increases with respect to k, in which the magnitude of the curves range from \sim 2 to 200. Conversely, the curves for the capacitance, as shown in Fig. 16, range from \sim 1 to \sim 0.2 where they decrease with increasing k. Furthermore, the curves for R_k increase in value with respect to α , while C_k decrease with respect to this parameter.

4. Discussion

4.1. Fluctuation modeling and analysis

As observed in Fig. 9, the amount of the stored energy in the capacitor increases with decreasing α . Hartley et al. derived a similar relationship for the energy gained on a fractional order capacitor exposed to a constant charging voltage [65]. As discussed earlier, the fractional exponent, α , corresponds to the degree of memory in the system, and can, thus, be thought of as a memory parameter. More specifically, as α tends toward 1, the scheme tends to reach a memoryless (Markovian) system [69,70]. Thus, as the memory of the capacitor system increases, the energy stored in the dielectric increases over time, as well.

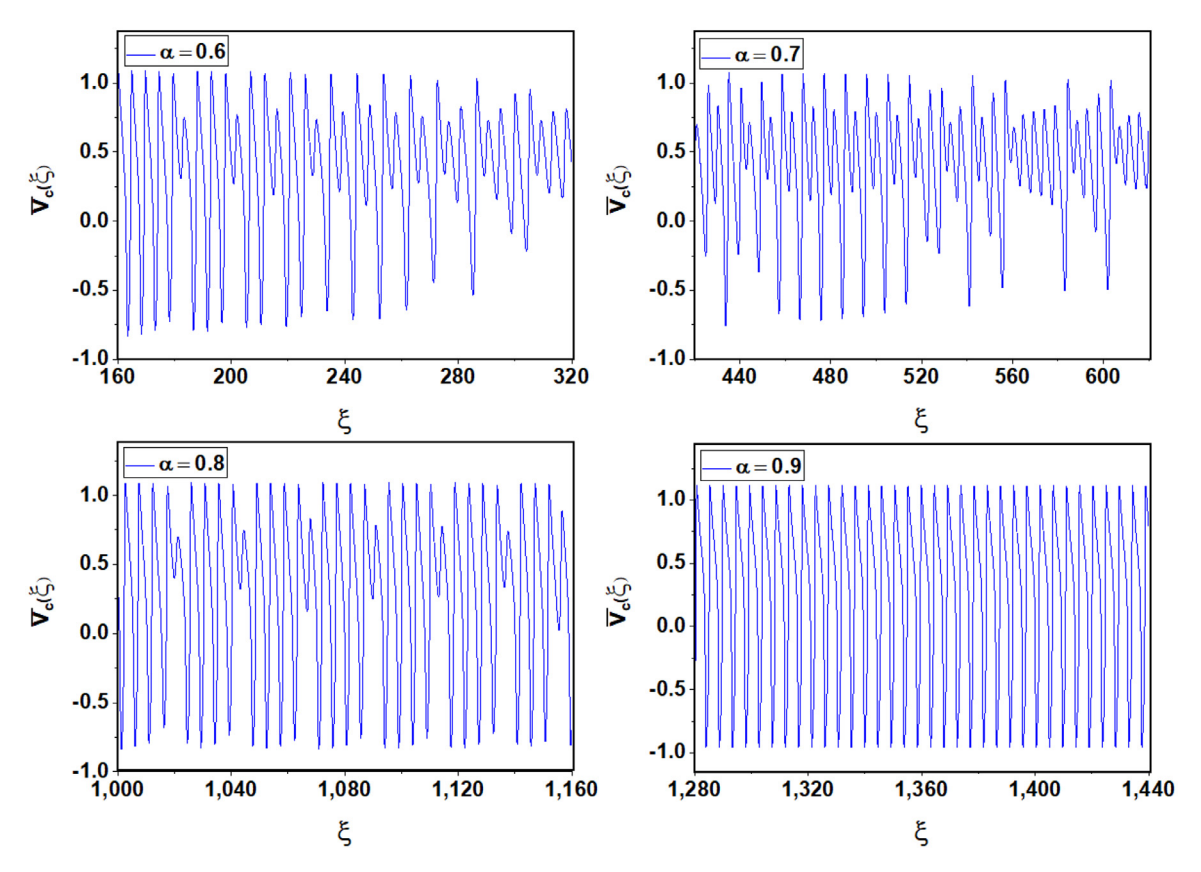


Fig. 13. Magnified regions of chaotic behavior (0.6 $< \alpha < 0.8$) and non-chaotic behavior for $\alpha = 0.9$ from Fig. 9 for $B_1 = 0.06$. (For the interpretation of the references to color in this figure legend, the reader is referred to the web version of this article.)

Westerlund suggested that the memory effect in a non-ideal capacitor is closely related to the dielectric absorption in the material [34]. He related this effect with the ability of the dielectric in the capacitor to "remember" previous voltages. This memory phenomenon was observed in experiments that involved an open capacitor that was previously charged and discharged for a predetermined set of time [26]. It was found that the potential curves increased in value when the fractional exponent corresponding to the dielectric decreased in value.

Further insight into the above phenomena can be gained by examining the types of dielectric materials used in the same study. The materials reported include polypropylene and polyvinylidene fluoride with fractional exponents of 0.999952 and 0.9776, respectively. As discussed previously, the decrease in the fractional exponent was linked to an increase in the relative permittivity, ε_r , of the dielectric. For this study, it was 2.2 for polypropylene and 11 for polyvinylidene, which indicates that the memory and the stored energy in the capacitor are linked to the polarizability of the constituent elements in the dielectric, and, hence, the microscopic makeup of the material.

A more explicit link between the energy stored on the capacitor and the memory of the system can be observed in the central integral of Eq. (49a). Here, the integrand involves the product of the time derivative of the potential and a power-law memory kernel with α as the exponent. Additionally, the potential is proportional to the applied electric field on the capacitor. Therefore, it can be thought that the amount of the electrostatic energy stored on the capacitor increases as its sensitivity to the past dynamical behavior of the field increases. In other words, an increased ability of the dielectric to "remember" past excitations result in a larger amount of the energy contained therein.

This interplay between the memory and the energy stored on the capacitor system can also be observed in Figs. 7 and 10. As can be observed in the graphs, the stored energy is the highest for $\alpha = 0.7$, where the oscillation death occurred in which the voltage values fluctuate the least. It is apparent that the most energy is stored when the oscillations are minimized. Moreover, the effects of memory on the stored energy can be seen in Eq. (49a), where the reduction in the energy arises from the integral taking account of the negative change in the voltage over time.

The implications of the behavior of the resistor and capacitor elements, as observed in Figs. 15 and 16, may be explained as follows. As α is decreased, the curves of the R_k 's decrease while those for the C_k 's increase. This relationship not only signifies an increase in the ability of the current to travel down the ladder, but also the degree in which the corresponding energy can be stored in each subsequent capacitor element. Since a decrease in α signifies an increase in the memory of

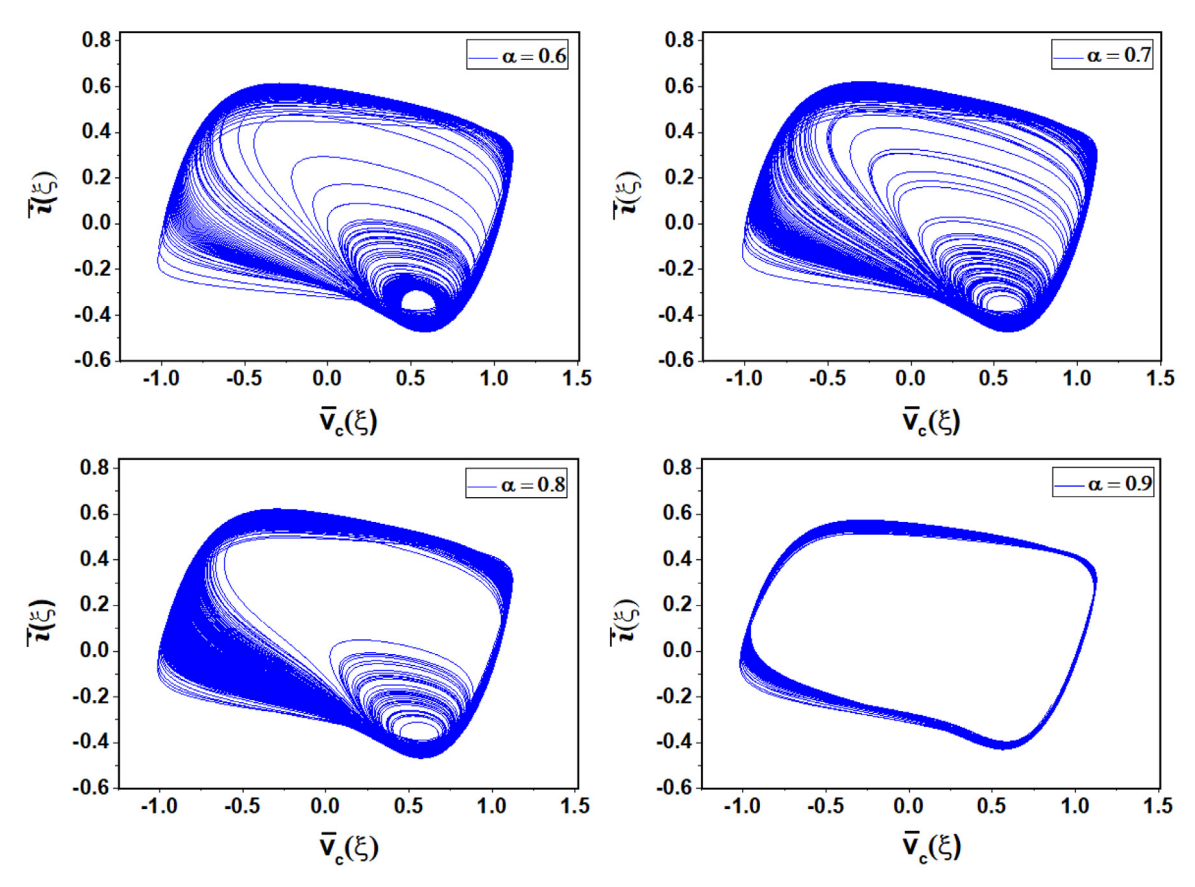


Fig. 14. Corresponding phase portraits for Fig. 9 (0.6 $< \alpha < 0.9$) and non-chaotic behavior from Fig. 9 for $B_1 = 0.06$. (For the interpretation of the references to color in this figure legend, the reader is referred to the web version of this article.)

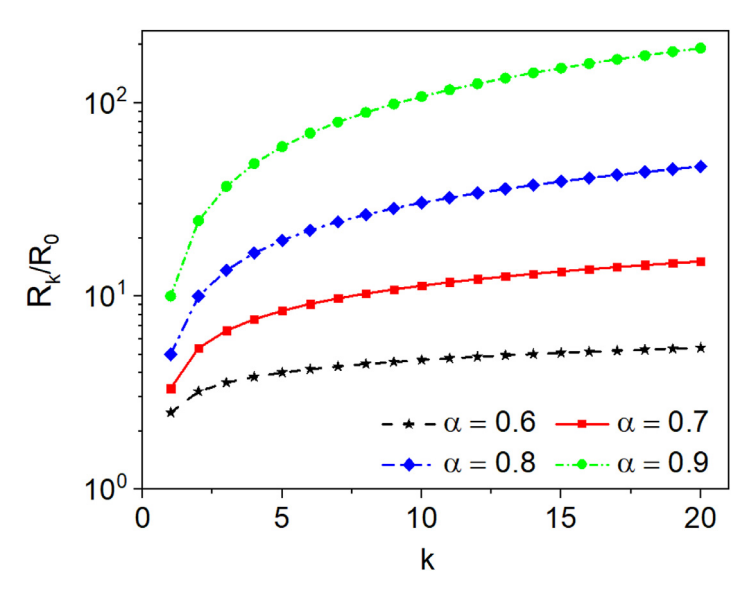


Fig. 15. Ratio of the *k*th resistor element to the initial resistor element, R_0 , from the ladder model plotted with respect to *k* for $0.6 < \alpha < 0.9$. (For the interpretation of the references to color in this figure legend, the reader is referred to the web version of this article.)

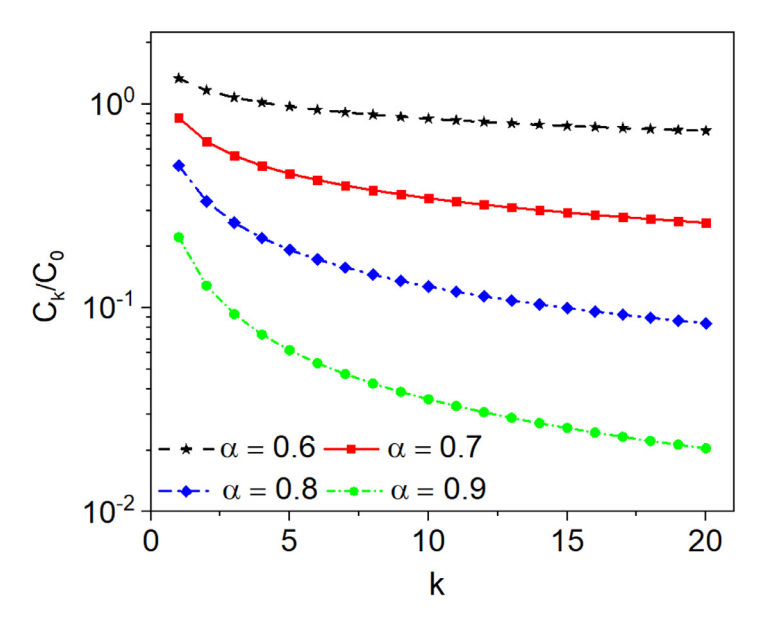


Fig. 16. Ratio of the *k*th capacitor element to the initial capacitor element, C_0 , from the ladder model plotted with respect to *k* for $0.6 < \alpha < 0.9$. (For the interpretation of the references to color in this figure legend, the reader is referred to the web version of this article.)

the system, the capacitor unit on the ladder may be thought of as a memory element in addition to a unit of the energy storage.

When $\alpha \to 0$, the R_k 's become negligible while the C_k 's become arbitrarily large (for k > 0). This behavior indicates that the current propagates down the ladder unimpeded, and the voltage on each capacitor element becomes vanishingly small due to the relation of C = q/V, where q is the charge. As a consequence, Ohm's law is recovered for the overall system where it behaves like a resistor. In this condition, the term, C_0 , represents the parasitic capacitance in the element [71].

On the other hand, as the fractional parameter trends toward 1, the resistance in each consecutive element grows at a faster rate with increasing k. In addition, the capacitance on each element, C_k , decreases in a similar fashion. In this sense, perhaps, a resistor element may be thought of as a memory negator via some type of dissipation mechanism. As can be observed in Eqs. (21) and (22), in the limit of $\alpha \to 1$, all R_k 's tend to infinity while all C_k 's become infinitesimally small. This trend symbolizes the inability of the current to traverse down the ladder to store energy in the individual capacitors, and thus the ladder becomes a simple capacitor where R_0 represents the equivalent series resistance.

When $B_1 = 0.06$, a decrease in α , and consequently an increase in the memory of the system, leads to an earlier onset of chaos, as observed in Fig. 12. The memory-induced chaos has also been observed in the cardiac excitation [72]. For the given parameters, therefore, a reduction in the memory of the system can delay the onset of dynamical instabilities in the potential across the capacitor. Perhaps the ability of the dielectric to remember earlier values may lead to greater sensitivity in initial conditions, which consequently induces chaos at earlier times. The reason for the greater degree of the erratic behavior for $\alpha = 0.7$, as compared to the other conditions (see Figs. 13 and 14) is not fully understood at this time, and, therefore, further work will be required to resolve this issue.

4.2. Thermal voltage noise analysis

The power density spectrum, $S_V(\omega)$ of the equilibrium voltage fluctuation on the real part of an impedance, $Z(\omega)$, according to the fluctuation-dissipation theorem, is given by [73]:

$$S_V(\omega) = 4k_B T Re\{Z(\omega)\} \tag{51}$$

where k_B is Boltzmann's constant, T is the temperature, h is the Planck's constant, and ω is the angular frequency of the oscillations. Using the universal dynamical theory, Teitler et al. [74] was able to derive the following spectral dependence:

$$S_V(\omega) \propto \frac{1}{\omega^{\alpha}}; \ 0 < \alpha < 1; \ \omega \gg \omega_p$$
 (52)

Since the exponent from Eq. (52) is the same as that used for the Curie-von Schweidler law, it is also equal to the exponent of the fractional derivative in the context of the present work. Therefore, it can also be said that the spectral dependence depends on the memory of the system. In the extreme cases, the voltage exhibits white noise fluctuations for $\alpha = 0$, while displaying the pink (flicker) noise behavior for $\alpha = 1$. In terms of the capacitor system, the pink noise is, thus, associated with a dielectric that is memoryless, while the white noise corresponds to one with the complete memory. Since

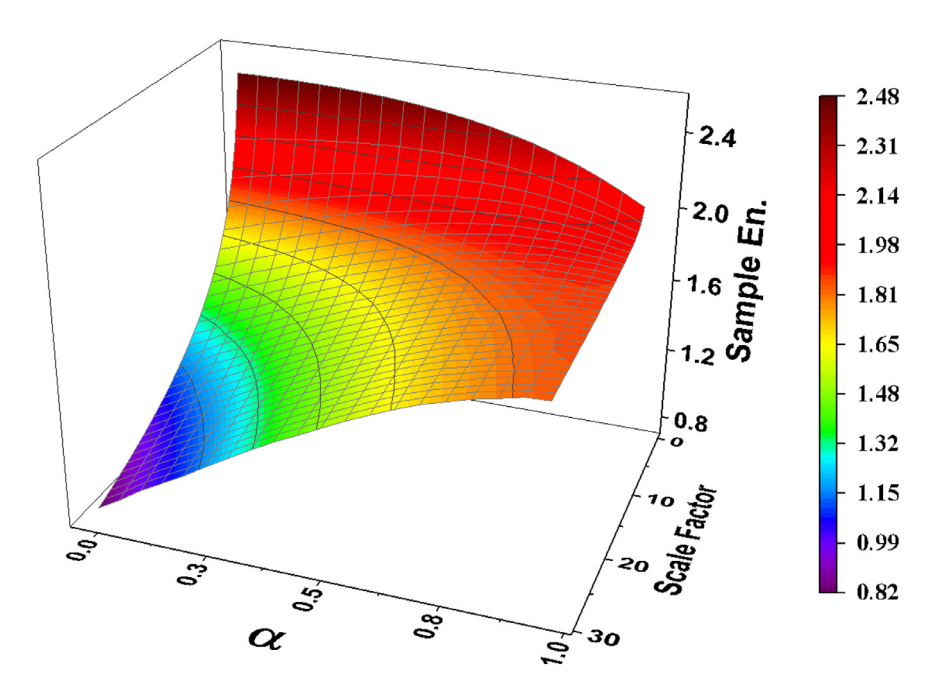


Fig. 17. Mean sample entropy of the colored noise data for $1 \le \tau \le 30$ plotted for $0 < \alpha < 1$ (from reference [67]). (For the interpretation of the references to color in this figure legend, the reader is referred to the web version of this article.)

this type of noise is associated with direct current [75], it will be assumed that this kind of behavior will only apply to the system when $V_1 = 0$ and the current has reached the steady-state condition.

Ngai et al. [74] suggested that the spectral exponent is affected by the microscopic configuration of the dielectric. For example, the exponent may change if the material has become more heterogenous over time due to an applied stress. Howell et al. found that α varied as a function of temperature in a study involving the dielectric relaxation of a glassforming material [76]. They hypothesized that the change in the decay behavior (varying α) arose from an increase in the microscopic heterogeneity with increasing temperature at constant pressure.

Brechtl et al. [77,78] previously examined the complexity of the $\frac{1}{\omega^{\alpha}}$ noise (also referred to as the colored noise) with exponents ranging from -2 to 2 using the refined composite multiscale entropy technique. As discussed in [79,80], the complexity is a measure of the degree of long-range correlations and intricacy of the dynamical behavior of a given system. To model and analyze the time series, using this method, the complexity metric is plotted with respect to the scale factor, which is used to coarse-grain the original time series. The complexity at a given scale factor is typically called the sample entropy value [79]. For series in which the sample entropy either increases or remains constant with an increasing scale factor, the series consists of long-range correlations.

Fig. 17 displays the sample entropy for the colored noise for α values ranging from 0 (white noise) to 1 (pink noise). As can be seen, the curves increase, overall, with an increase in the above parameter. Additionally, the sample-entropy goes from a strictly-decreasing function at $\alpha=0$ to remaining practically constant at $\alpha=1$. What is also evident from the graph is that there is a spectrum of sample-entropy curves with respect to the exponent, α . Using the above ideas, it can, therefore, be said that the degree of long-range correlations in the colored noise increases in a continuous fashion as the spectral exponent rises in value.

Now we will examine the behavior of a capacitor which contains a liquid dielectric. In this context, the dielectric will be composed of charge carriers instead of dipolar elements, where α ranges from 0.6 to 0.95 [37]. For this system, the motion of the carriers will be governed by the Langevin equation subject to a stochastic (colored noise) force. This force will result from the bombardment of the carrier by the molecules or ions of the electrolyte [75]. Monnai et al. examined the effect of the spatio-temporal colored noise on the diffusive nature of a particle in a potential well [81]. It was determined that an increase in the spatial correlations of the noise corresponded to a decrease in the drift velocity of the particle. Conversely, it can be thought that a decrease in the spatial correlations leads to an increase in the same velocity.

Based on the discussion above, it can be thought that the degree of long-range correlations of the voltage noise decreases with respect to the fractional parameter. Assuming these types of correlations have a spatial component, it will be suggested here that the drift velocity of the charge carriers will increase as α decreases. Since the drift velocity is proportional to the conductance of the media, the above hypothesis suggests that the dielectric becomes more "metal-like" as the exponent decreases [34]. With respect to the ladder model, the decrease in the resistances, R_k , with decreasing α , can be thought of as an analogue for this type of behavior.

It should also be mentioned that in [81], they determined that the spatial correlations were positively correlated with the Gaussian memory. The above finding is in contrast with the present work, where a higher amount of complexity in the voltage fluctuations was associated with a lower degree of memory. The link between the increase in the memory of the non-ideal capacitor and the decrease in the complexity of voltage fluctuations is not entirely understood and, therefore, should be explored in the future.

The decrease in the complexity of the noise may be due to an increase in the degree of inherent randomness in the system [82]. This increased randomness may be linked to the increased drift velocity of the carriers, where the behavior is assumed to be more erratic in nature. Thus, it may be said that an increasing metallic character corresponds to a decrease in the complexity of the noise fluctuations. In addition, if it is assumed that the level of impurities in the material remains constant, then an increase in the mobility leads to a rise in the trapping length [83]. Consequently, the interaction between the carriers and the impurities is decreased. A decrease in the amount of possible interactions in a dynamical system has been linked to the reduction in the complexity of the system behavior [84].

5. Conclusions

For the present work, the potential fluctuations of the Bonhoeffer van der Pol oscillator system with a non-ideal capacitor was investigated, using a fractional differential equation model. It was found that the order of the fractional derivative, α , is also a measure of the memory in the dielectric. Furthermore, it was found that the dynamical behavior of the potential across the capacitor was affected by this parameter, and, therefore, the memory of the system. Importantly, findings indicate that an increase in the memory was associated with an increase in the energy stored in the dielectric. Therefore, it can be theorized that the fractional derivative may also be some type of function of the stored energy, although the underlying reasons for this trend are not fully understood. Furthermore, the effects of the dynamical behavior on the capacity of the dielectric to store energy were observed. Here, fluctuations that exhibited the oscillation death led to more energy being stored in the dielectric, as compared to the behavior, which displayed relaxation oscillations and chaotic behavior. The relatively-lower stored energy resulting from the latter types of oscillations is accounted for by the memory effect, where the present accumulation of energy is affected by previous decreases in the potential across the component. Thus, the dielectric material "remembers" the past behavior of the voltage, which result in either a decrease or an enhancement in the stored energy. In addition, the effect of the history of the voltages across the capacitor was apparent where the fluctuation exhibiting the oscillation death led to the highest amount of energy stored on the capacitor, as compared to the other conditions after enough time had elapse. Moreover, an increase in α , under certain conditions, led to the earlier onset of chaotic voltage oscillations across the capacitor. It is suggested here that perhaps an increase in the memory of the system causes the behavior to be more sensitive to its initial state, which results in erratic fluctuations at earlier times. Additionally, the corresponding phase portraits showed that the chaotic behavior was enhanced, in general, with a decrease in α . In addition, it was found that the non-ideal capacitor has a transitory nature, where it becomes more like a resistor as $\alpha \to 0$, and conversely, more like a capacitor as $\alpha \to 1$. Furthermore, a decrease in α was linked to an enhanced metallic character of the dielectric due to the charge-carrier analogy. This change was thought to be caused by an increase in the drift velocity due to the decrease in the long-range correlations of the thermal voltage noise.

Acknowledgments

We gratefully acknowledge the support of the US National Science Foundation (NSF) through grants DMR 1611180 and 1809640, the Department of Energy (DOE), DE-FE-00011194 (PKL and XX) with Drs. Shiflet, Farkas, Cedro, and Mullen as contract monitors. Financial support for JB was provided using Univ. Tennessee discretionary research funds provided by Dr. S.J. Zinkle. The authors would also like to thank Dr. Shakoor Pooseh for helpful discussions concerning the implementation of the fractional differential equation algorithm.

References

- [1] Stratonovich RS. Topics in the Theory of Random Noise, New York, Gordon and Breach; 1967.
- [2] Nayfeh AH. Nonlinear Oscillations, Pure and Applied Mathematics. second ed. New York, Wiley; 2008.
- [3] Haken H. Cooperative phenomena in systems far from thermal equilibrium and in nonphysical systems. Rev. Mod. Phys 1975;47:67–121.
- [4] Hanggi P, Riseborough P. Dynamics of non-linear dissipative oscillators. Am. J. Phys 1983;51:347–52.
- [5] Brechtl J, Chen SY, Xie X, Ren Y, Qiao JW, Liaw PK, et al. Towards a greater understanding of serrated flows in an Al-containing high-entropy-based alloy. Int. J. Plast 2018. doi:10.1016/j.ijplas.2018.11.011.
- [6] Chen S, Li W, Xie X, Brechtl J, Chen B, Li P, et al. Nanoscale serration and creep characteristics of Al_{0.5}CoCrCuFeNi high-entropy alloys. J. Alloys Compds 2018;752:464–75.
- [7] Chen S, Yu L, Ren J, Xie X, Li X, Xu Y, et al. Self-similar random process and chaotic behavior in serrated flow of high entropy alloys. Sci. Rep 2016;6:29798.
- [8] Pol BVd. A theory of the amplitude of free and forced triode vibrations. Radio Rev 1920;1:54-62 701-10.
- [9] Strogatz SH. Nonlinear Gynamics and Chaos With Applications to Physics, Biology, Chemistry, and Engineering. Cambridge: Perseus Books Publishing, LLC; 1994.
- [10] Rajasekar S, Lakshmanan M. Period doubling route to chaos for a BVP oscillator with periodic external force. J Theory Biol. 1988;133:473-7.
- [11] Rabinovitch A, Thieberger R, Friedman M. Forced Bonhoeffer-Van Der Pol oscillator in its excited mode. Phys. Rev. E. 1994;50:1572-8.
- [12] Kurrer C, Schulten K. Effect of noise and perturbations on limit cycle systems. Phys. D. 1991;50:311–20.
- [13] Nomura T, Sato S, Doi SJ, Segundo JP, Stiber MD. Global bifurcation structure of a Bonhoeffer-Van Der Pol oscillator driven by periodic pulse trains comparison with data from a periodically inhibited biological pacemaker. Biol. Cybern 1994;72:55–67.

- [14] Nagumo J, Arimoto S, Yoshizawa S. Active pulse transmission line simulating nerve axon. Proc. Inst. Radio Eng 1962;50:2061.
- [15] Kousaka T, Ogura Y, Shimizu K, Asahara H, Inaba N. Analysis of mixed-mode oscillation-incrementing bifurcations generated in a nonautonomous constrained Bonhoeffer-Van Der Pol oscillator. Phys. D-Nonlinear Phenom 2017;353:48–57.
- [16] Rossler OE, Wegmann K. Chaos in the Zhabotinskii reaction. Nature 1978;271:89.
- [17] Gyorgyi L, Field RJ. A 3-variable model of deterministic chaos in the Belousov-Zhabotinsky reaction. Nature 1992;355:808-10.
- [18] Janson NB, Marsden CJ. Dynamical system with plastic self-organized velocity field as an alternative conceptual model of a cognitive system. Sci. Rep 2017:7:17007.
- [19] Ramesh M, Narayanan S. Chaos control of Bonhoeffer-Van Der Pol oscillator using neural networks. Chaos Solitons Fractals 2001;12:2395-405.
- [20] Shimizu K, Saito Y, Sekikawa M, Inaba N. Complex mixed-mode oscillations in a Bonhoeffer-Van Der Pot oscillator under weak periodic perturbation. Phys.D-Nonlinear Phenom 2012;241:1518–26.
- [21] Kutafina E. Mixed mode oscillations in the Bonhoeffer-Van Der Pol oscillator with weak periodic perturbation, Comput. Appl. Math 2015;34:81–92.
- [22] Hudson JL, Hart M, Marinko D. Experimental-study of multiple peak periodic and nonperiodic oscillations in the Belousov-Zhabotinskii reaction. J. Chem. Phys. 1979;71:1601–16.
- [23] Petrov V, Scott SK, Showalter K. Mixed-mode oscillations in chemical-systems. J. Chem. Phys. 1992;97:6191-8.
- [24] Schell M. Albahadily FN. Mixed-mode oscillations in an electrochemical system .2. A periodic chaotic sequence. I. Chem. Phys. 1989:90:822-8.
- [25] Drover J, Rubin J, Su JH, Ermentrout B. Analysis of a canard mechanism by which excitatory synaptic coupling can synchronize neurons at low firing frequencies. SIAM J. Appl. Math 2004;65:69–92.
- [26] Westerlund S, Ekstam L. Capacitor theory. IEEE Trans Dielectr. Electr. Insul. 1994;1:826-39.
- [27] Jonscher AK. The 'universal' dielectric response. Nature 1977;267:673.
- [28] Curie, MJ. Recherches sur la conductibilit des corps cristallises, Ann. Chim. Phys. 6(1889) 203-269.
- [29] Oldham KB, Spanier J. The Fractional Calculus. New York: Dover Publications; 2002.
- [30] Miller KS, Ross B. An Introduction to the Fractional Calculus and Fractional Differential Equations. New York: Wiley & Sons, Inc.; 1993.
- [31] Tarasov VE. Quantum dissipation from power-law memory. Ann. Phys. 2012;327:1719-29.
- [32] Caputo M, Mainardi F. New dissipation model based on memory mechanism. Pure Appl. Geophys 1971;91:134.
- [33] Caputo M, Mainardi F. Linear models of dissipations in anelastic solids. Riv. Nuovo Cimento 1971;1:161-98.
- [34] Westerlund S. Dead matter has memory!. Phys. Scr. 1991;43:174-9.
- [35] Weinberg SH. Membrane capacitive memory alters spiking in neurons described by the fractional-order Hodgkin-Huxley model. PLoS One 2015;10:27.
- [36] Sarafraz MS, Tavazoei MS. Realizability of fractional-order impedances by passive electrical networks composed of a fractional capacitor and RLC components. IEEE Trans. Circuits Syst. I-Regul. Pap 2015;62:2829–35.
- [37] Jonscher AK. Hopping losses in polarizable dielectric media. Nature 1974;250:191–3.
- [38] Schiessel H, Blumen A. Hierarchical analogs to fractional relaxation equations. J. Phys. A-Math Gen 1993;26:5057-69.
- [39] Heymans N. Constitutive equations for polymer viscoelasticity derived from hierarchical models in cases of failure of time-temperature superposition. Signal Process 2003;83:2345–57.
- [40] Heymans N, Bauwens JC. Fractal rheological models and fractional differential-equations for viscoelastic behavior. Rheol. Acta 1994;33:210-19.
- [41] Nadzharyan TA, Sorokin VV, Stepanov GV, Bogolyubov AN, Kramarenko EY. A fractional calculus approach to modeling rheological behavior of soft magnetic elastomers. Polymer 2016;92:179–88.
- [42] Bagley RL. The thermorheologically complex material. Int. J. Eng. Sci 1991;29:797-806.
- [43] Tarasov VE. Path integral for quantum operations. , J. Phys. A-Math Gen. 2004;37:3241-57.
- [44] Laskin N. Fractional quantum mechanics and levy path integrals. Phys. Lett. A. 2000;268:298-305.
- [45] Oldham KB, Spanier J. The replacement of Fick's laws by a formulation involving semidifferentiation. J. Electroanal. Chem. Interfacial Electrochem 1970;26:331–41.
- [46] Bologna M, Tsallis C, Grigolini P. Anomalous diffusion associated with nonlinear fractional derivative Fokker-Planck-like equation: exact time-dependent solutions. Phys. Rev. E. 2000;62:2213–18.
- [47] Zolotarev VM, Uchaikin VV, Saenko VV. Superdiffusion and stable laws. J. Exp. Theoret. Phys. 1999;88:780–7.
- [48] Tarasov VE, Zaslavsky GM. Fractional dynamics of systems with long-range space interaction and temporal memory. Phys.-Stat. Mech. Appl 2007;383:291–308.
- [49] Gafiychuk V, Datsko B, Meleshko V. Analysis of fractional order Bonhoeffer-Van Der Pol oscillator. Phys. A-Stat. Mech. Appl 2008;387:418–24.
- [50] Sekikawa M, Shimizu K, Inaba N, Kita H, Endo T, Fujimoto K, et al. Sudden change from chaos to oscillation death in the Bonhoeffer-Van Der Pol oscillator under weak periodic perturbation. Phys. Rev. E. 2011;84:8.
- [51] Zhong GQ. Implementation of Chuas circuit with a cubic nonlinearity. IEEE Trans. Circuits Syst. I-Fundam. Theoret. Appl. 1994;41:934-41.
- [52] Schweidler ERv. Studies on the anomalous behaviour of dielectrics. Ann. Phys 1907;329:711-70.
- [53] Alioto M, Palumbo G, Poli M. Evaluation of energy consumption in RC ladder circuits driven by a ramp input. IEEE Trans. Very Large Scale Integr. (VLSI) Syst. 2004;12:1094–107.
- [54] Nelms RM, Cahela DR, Tatarckuk BJ. Modeling double-layer capacitor behavior using ladder circuits. IEEE Trans. Aerosp. Electron Syst 2003;39:430-8.
- [55] Kelly JF, McGough RJ. Fractal ladder models and power law wave equations. J. Acoust. Soc. Am. 2009;126:2072–81.
- [56] Roy SCD. On realization of a constant-argument immittance or fractional operator. IEEE Trans. Circuit Theory 1967; CT14:264.
- [57] Cuyt A, Petersen V, Verdonk B, Waadeland H, Jones W. Handbook of Continued Fractions for Special Functions. New York: Springer; 2008.
- [58] Almeida R, Pooseh S, Torres DFN. Computational Methods in the Fractional Calculus of Variations. London: Imperial College Press; 2015.
- [59] Pooseh S, Almeida R, Torres DFM. Approximation of fractional integrals by means of derivatives. Comput. Math. Appl 2012;64:3090-100.
- [60] Almeida R, Pooseh S, Torres DFM. Computational Methods in the Fractional Calculus of Variations. Imperial College Press; 2015.
- [61] Gottwald GA, Melbourne I. Testing for chaos in deterministic systems with noise. Phys. D-Nonlinear Phenom 2005;212:100–10.
- [62] Cafagna D, Grassi G. Bifurcation and chaos in the fractional-order Chen system via a time-domain approach. Int. J. Bifurcation Chaos. 2008;18:1845–63.
- [63] Cafagna D, Grassi G. An effective method for detecting chaos in fractional-order systems. Int. J. Bifurcation Chaos. 2010;20:669-78.
- [64] Mainardi F. Fractional Calculus and Waves in Linear Viscoelasticity: An Introduction to Mathematical Models. London: Imperial College Press; 2010.
- [65] Hartley TT, Veillette RJ, Adams JL, Lorenzo CF. Energy storage and loss in fractional-order circuit elements. IET Circuits Devices Syst. 2015;9:227-35.
- [66] Gray PR, Hurse PJ, Lewis SH, Meyer RG. Analysis and Design of Analog Integrated Circuits. fifth ed. New York: Wiley; 2009.
- [67] Kepler RG, Coppage FN. Generation and recombination of holes and electrons in anthracene. Phys. Rev 1966;151:610-14.
- [68] Agarwal VK, Ichijo B. Determination of dielectric-constant of stearic-acid films using varying gap immersion method. Electrocomponent Sci. Technol 1977;4:23–8.
- [69] West BJ, Bologna M, Grigolini P. Physics of Fractal Operators. New York: Springer; 2003.
- [70] Saeedian M, Khalighi M, Azimi-Tafreshi N, Jafari GR, Ausloos M. Memory effects on epidemic evolution: the susceptible-infected-recovered epidemic model. Phys. Rev. E. 2017:95:9.
- [71] Demurie SN, Demey G. Parasitic capacitance effects of planar resistors. IEEE Trans. Components Hybrids Manuf. Technol 1989;12:348-51.
- [72] Landaw J, Garfinkel A, Weiss JN, Qu Z. Memory-induced chaos in cardiac excitation. Phys. Rev. Lett 2017;118:5.
- [73] Galeczki G, Hajdu J, Kiss LB. Note on the interrelation between low-frequency dielectric response and 1/f noise in condensed matter systems. Solid State Commun 1989;72:1131–3.
- [74] Teitler S, Ngai KL. A diagnostic for the condition of dielectrics. IEEE Trans. Electr. Insul 1981;16:414-16.
- [75] Ngai KL. Unified theory of 1-f noise and dielectric response in condensed matter. Phys. Rev. B. 1980;22:2066-77.
- [76] Howell FS, Bose RA, Macedo PB, Moynihan CT. Electrical relaxation in a glass-forming molten-salt. J. Phys. Chem. 1974;78:639-48.

- [77] Wu S-D, Wu C-W, Lin S-G, Lee K-Y, Peng C-K. Analysis of complex time series using refined composite multiscale entropy. Phys.Lett. A. 2014;378:1369-74.
- [78] Brechtl J, Xie X, Liaw PK, Zinkle SJ. Complexity modeling and analysis of chaos and other fluctuating phenomena. Chaos, Solitons Fractals 2018;116:166-75.
- [79] Costa M, Goldberger AL, Peng CK. Multiscale entropy analysis of complex physiologic time series. Phys. Rev. Lett 2002;89:068102.
- [80] Pincus SM. Approximate entropy as a measure of system complexity. Proc. Natl. Acad. Sci. 1991;88:2297–301.
 [81] Monnai T, Sugita A, Nakamura K. Diffusion in the Markovian limit of the spatio-temporal colored noise. Epl. 2008;84:5.
- [82] Costa M, Goldberger AL, Peng CK. Multiscale entropy analysis of biological signals. Phys. Rev. E. 2005;71:021906.
- [83] Arino-Estrada G, Chmeissani M, de Lorenzo G, Kolstein M, Puigdengoles C, Garcia J, et al. Measurement of mobility and lifetime of electrons and holes in a Schottky CDTE diode. J. Instrum 2014;9:7.
- [84] Sarkar A, Chatterjee A, Barat P, Mukherjee P. Comparative study of the Portevin-Le Chatelier effect in interstitial and substitutional alloy. Mater. Sci. Eng. A 2007;459:361-5.